A Unified Convection Scheme (UNICON). Part I: Formulation

SUNGSU PARK

Climate and Global Dynamics Division, National Center for Atmospheric Research, Boulder, Colorado

(Manuscript received 30 July 2013, in final form 27 May 2014)

ABSTRACT

The author develops a unified convection scheme (UNICON) that parameterizes relative (i.e., with respect to the grid-mean vertical flow) subgrid vertical transport by nonlocal asymmetric turbulent eddies. UNICON is a process-based model of subgrid convective plumes and mesoscale organized flow without relying on any quasi-equilibrium assumptions such as convective available potential energy (CAPE) or convective inhibition (CIN) closures. In combination with a relative subgrid vertical transport scheme by local symmetric turbulent eddies and a grid-scale advection scheme, UNICON simulates vertical transport of water species and conservative scalars without double counting at any horizontal resolution.

UNICON simulates all dry–moist, forced–free, and shallow–deep convection within a single framework in a seamless, consistent, and unified way. It diagnoses the vertical profiles of the macrophysics (fractional area, plume radius, and number density) as well as the microphysics (production and evaporation rates of convective precipitation) and the dynamics (mass flux and vertical velocity) of multiple convective updraft and downdraft plumes. UNICON also prognoses subgrid cold pool and mesoscale organized flow within the planetary boundary layer (PBL) that is forced by evaporation of convective precipitation and accompanying convective downdrafts but damped by surface flux and entrainment at the PBL top. The combined subgrid parameterization of diagnostic convective updraft and downdraft plumes, prognostic subgrid mesoscale organized flow, and the feedback among them remedies the weakness of conventional quasi-steady diagnostic plume models—the lack of plume memory across the time step—allowing UNICON to successfully simulate various transitional phenomena associated with convection (e.g., the diurnal cycle of precipitation and the Madden–Julian oscillation).

1. Introduction

In any atmospheric model, three separate schemes—advection, PBL, and convection—perform vertical transport of water species and conservative scalars: the advection scheme achieves this through the resolved grid-mean flow, while the PBL and convection schemes perform vertical transport through the parameterized subgrid turbulent eddies. Ideally, the sum of vertical transport from these three schemes over a fixed geographical domain (e.g., the whole Earth) should be invariant to the changes of the horizontal grid size of the model, $G \equiv \Delta x \Delta y$, where Δx and Δy are the zonal and meridional width of the model grid, respectively. If the advection scheme accurately simulates grid-mean flow in various G, then a set of sufficient and necessary conditions to achieve this scale adaptivity is that 1) both PBL and convection schemes are designed to parameterize relative subgrid motion with respect to the resolved grid-mean flow, 2) the relative subgrid motion parameterized by the convection scheme is completely separated from that parameterized by the PBL scheme, and 3) the PBL and convection schemes should be able to parameterize the entire relative subgrid motion together. Any atmospheric models failing to meet these conditions will result in poor scale adaptivity due to missing or double-counted vertical transport. Developing an appropriate convection scheme is the most challenging but essential task necessary to develop a suite of scale-adaptive physics parameterizations for future atmospheric models.

In some atmospheric models, subgrid vertical transport by unsaturated dry convection has been parameterized as a nonlocal transport term within the PBL scheme (e.g., Holtslag and Boville 1993). Saturated moist convection above the PBL top that is typically located just below the lifting condensation level (LCL) of a convective updraft plume (Fig. 1a) is treated in a

Corresponding author address: Sungsu Park, Climate and Global Dynamics Division, National Center for Atmospheric Research, P.O. Box 3000, Boulder, CO 80307.
E-mail: sungsup@ucar.edu

DOI: 10.1175/JAS-D-13-0233.1

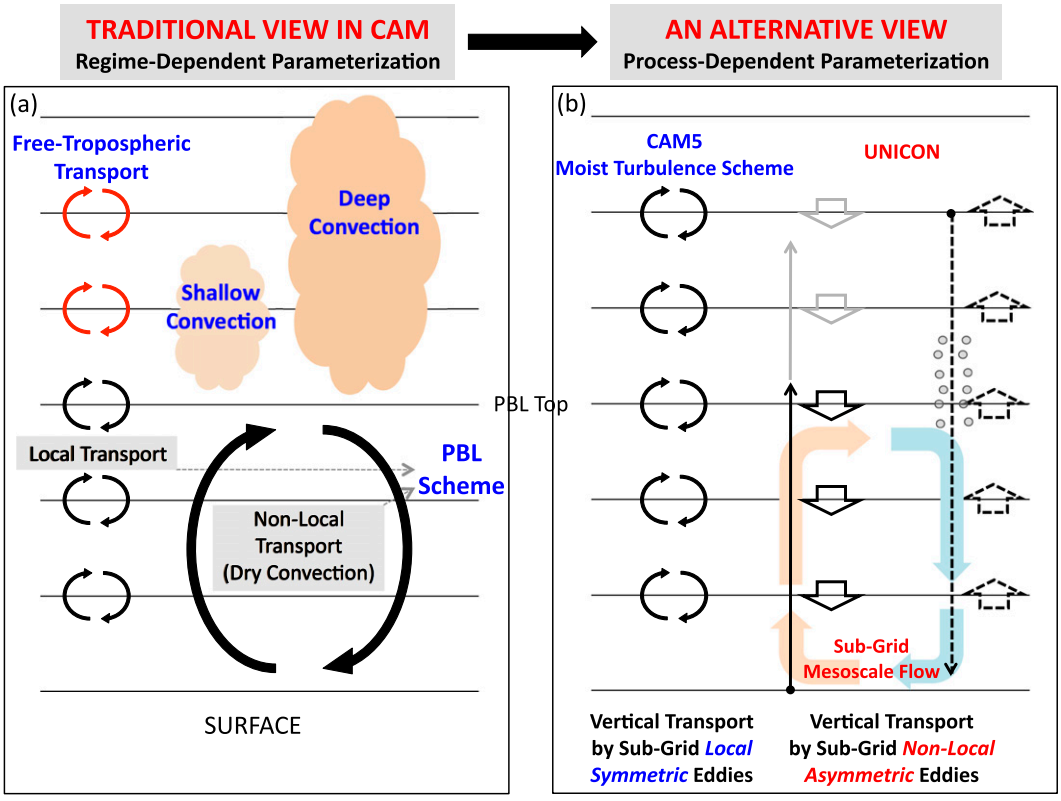

FIG. 1. Diagrams illustrating subgrid vertical transport in atmospheric models with (a) the traditional view in CAM and (b) the alternative view that is adopted by UNICON with CAM5. In the traditional regime-dependent parameterization, subgrid vertical transport within the PBL is performed by the PBL scheme consisting of local and (dry) nonlocal transport terms driven by surface buoyancy flux. Above the PBL, local transport at each level is parameterized by a specific function of the local Richardson number independent from that used in the PBL scheme (i.e., free-tropospheric transport), while nonlocal transport is parameterized by saturated shallow and deep convection schemes. In the alternative process-dependent parameterization, local transport is parameterized by a moist turbulence scheme in CAM5 that simulates both dry and saturated turbulent transport in the entire atmospheric layers with a single set of moist physics formulas. The remaining nonlocal transport is performed by UNICON that consists of subgrid convective updrafts originated from the surface, typically in an unsaturated state, but that eventually become saturated above the LCL (thin upward-pointing solid arrow with black (dry) and gray (saturated) colors, with corresponding compensating subsidence denoted by thick downward-pointing solid arrow); subgrid convective downdrafts that are generated from convective updrafts and can penetrate into the PBL when sufficiently cooled by evaporation of convective precipitation (thin downward-pointing dashed arrow with corresponding compensating upwelling denoted by thick upward-pointing dashed arrow); and subgrid mesoscale organized flow driven by convective downdrafts and evaporation of convective precipitation, which feeds back to convective updrafts. In each plot, the black horizontal lines denote the model interfaces.

separate convection scheme. However, at least in the case of shallow convection, cumulus growing above the PBL is merely a visible identity of the underlying dry convective plume without abrupt changes of thermodynamic properties at the moment of saturation. Thus, it appears to be more reasonable to simulate both the dry and moist convection within a single convection scheme rather than simulating in separate PBL and convection schemes. An approach in line with this philosophy is an eddy diffusivity–mass flux model (Siebesma et al. 2007).

Over the continents, substantial portions of observed cumuli are negatively buoyant with little vertical extent above the PBL; that is, a dry convective updraft reaches its LCL but not its level of free convection (LFC). This forced convection has been neglected in the existing convection schemes (although some types of high-order turbulence closure models are capable of simulating the forced convection, if sophisticated), since both the CAPE and convective inhibition (CIN) closures are designed to simulate only the strong convective updrafts growing above the LFC (i.e., free convection). The forced convection, however, can foster subsequent free convection because, when detrained, it moistens environmental air near the PBL top. Any convection scheme without

appropriate treatment of forced convection is likely to have trouble in simulating the correct onset of free convection.

During the last half century, the convection parameterization community has developed various deep and shallow convection schemes. In order to close the model, Kuo (1965, 1974) and Tiedtke (1989) used the grid-scale moisture convergence for deep convection and the surface evaporation for shallow convection. Conceptually, Arakawa and Schubert (1974) and Emanuel (1991) can represent cumulus with various cloud tops including both deep and shallow convection. However, their closures (using the cloud work function, or CAPE, assuming a quasi equilibrium between grid-scale destabilization and subgrid convective stabilization) are not suitable for simulating shallow convection with small vertical extent confined within the lower troposphere. A deep convection scheme developed by Zhang and McFarlane (1995) uses a similar CAPE closure. Park and Bretherton (2009, hereafter PB09) developed a shallow convection scheme for general circulation models (GCMs) in which CIN rather than CAPE is used to compute updraft mass flux at the PBL top. In nature, a seamless transition from shallow to deep convection widely occurs both in space and time. In the trade wind regimes over the subtropical oceans west of the major continents, a continuous spectrum of cumulus is observed from nonprecipitating shallow cumulus [defined as CL1 where CL is a low-level cloud code used by surface observers defined from WMO (1975); see also Park and Leovy (2004)] in the upstream, to moderate cumulus (defined as CL2) and eventually precipitating deep cumulus (defined as CL3,9) in the far downstream (Hahn and Warren 1999). Over summertime continents, we frequently observe nonprecipitating bright narrow shallow cumulus until early afternoon but precipitating dark wide deep cumulus in late afternoon. It is likely that this seamless transition from shallow to deep cumulus in nature cannot be adequately simulated by separate shallow and deep convection schemes. Recently, Hohenegger and Bretherton (2011) and Mapes and Neale (2011) explored simulating deep convection by extending the shallow convection scheme developed by PB09.

Despite the aforementioned conceptual flaws, traditional convective parameterizations have made a tremendous contribution in improving our understanding of atmospheric convection. However, the performance of existing convection schemes is still far from reality. Some examples of convection-related problems in current GCMs are a double intertropical convergence zone (ITCZ) along the eastern equatorial Pacific ocean, too-frequent surface precipitation, grid storms (Williamson 2013), wrong phase and weak amplitude of the diurnal cycle of precipitation over the summer continents, weak or missing Madden–Julian oscillation (Madden and Julian 1971; Moncrieff et al. 2012), monsoon simulation over the western Pacific warm pool region, characteristics of El Niño–Southern Oscillation (ENSO), simulation of tropical cyclones, too-rapid transition from stratocumulus to cumulus in the subtropical oceans (Park et al. 2014), climate sensitivities of marine stratocumulus and cirrus, and simulation of aerosol indirect effects. These problems reflect that convection processes in nature are much more complex than those captured by existing convection schemes with various space and time scales. Some GCMs showed progress in suppressing the double ITCZ (Song and Zhang 2009; Chikira and Sugiyama 2010; Watanabe et al. 2010) or simulating the MJO (Kim et al. 2009; Chikira and Sugiyama 2013). However, addressing these issues in a synthetic way without degrading the other features remains a significant challenge.

In order to address the issues mentioned above both qualitatively and quantitatively, the author develops a unified convection scheme (UNICON)—a relative subgrid vertical transport scheme by nonlocal asymmetric turbulent eddies (Fig. 1b). UNICON is designed to simulate all dry–moist, forced–free, and shallow–deep convection within a single framework in a seamless, consistent, and unified way. UNICON is a process-based model of subgrid convective updraft and downdraft plumes and mesoscale organized flow without relying on any equilibrium assumptions, such as CAPE and CIN closures. It diagnoses the macrophysics (i.e., fractional area, plume radius, and number density) as well as the microphysics (i.e., production and evaporation rates of convective precipitation) and the dynamics (i.e., mass flux and vertical velocity) of multiple convective updraft and downdraft plumes, which are constructed on the prognosed subgrid cold pool and mesoscale organized flow within the PBL. As a consequence of the strict requirement on interprocess consistency, UNICON has unique treatments of the source air properties of convective updrafts and downdrafts, mixing processes between convective plumes and environment (or detrained air), downdraft dynamics, cold pool, and thermodynamic feedback among convective updrafts, downdrafts, and mesoscale organized flow. Without the closures assuming a certain equilibrium, UNICON is more physically oriented than the existing convection schemes, capable of simulating atmospheric variabilities in a flexible way at various space and time scales in a wide range of G. Arakawa and Wu (2013) proposed a conceptual method to develop a scale-adaptive convection scheme by allowing the convective updraft fractional area $\hat{A}$ to approach 1 as G decreases. However, thanks to the detailed dynamic treatment of subgrid convective updraft and

downdraft plumes and mesoscale organized flow without relying on the quasi-equilibrium assumption, UNICON in principle can achieve this scale adaptivity by retaining $\hat{A} \ll 1$ within the framework of the diagnostic plume model.

The structure of this paper is as follows. Section 2a provides a set of primitive governing equations from which a set of simplified diagnostic plume equations are derived, based on three fundamental assumptions that will be detailed. Sections 2b and 2c describe a specific parameterization of individual convective updraft and downdraft processes. Section 2d treats the parameterization of cold pool within the PBL, which drives subgrid mesoscale organized flow that feedbacks to convective updrafts, as will be detailed in section 2e. Section 2f explains how to compute sources within the environment. A summary and discussion is provided in section 3.

2. Model description

a. Governing equations

Consider a set of horizontally nonoverlapped convective updraft and convective downdraft plumes with fractional areas of $\hat{a}^i$ and $\check{a}^j$, respectively, embedded in an environment with fractional area of $\tilde{a} = 1 - \sum_i \hat{a}^i - \sum_j \check{a}^j$ in each layer. Here, superscripts hat ($\hat{a}$), check ($\check{a}$), and tilde ($\tilde{a}$) denote convective updraft, downdraft, and environment, respectively, and the indices i and j denote individual components of convective updrafts and downdrafts. Later, superscripts breve ($\breve{a}$) and double dots ($\ddot{a}$) will also be used to denote the values of the convective precipitation and evaporation areas, respectively. Each area has total vertical velocity ($\hat{w}_o$, $\check{w}_o$, $\tilde{w}_o$) and scalars ($\hat{\phi}$, $\check{\phi}$, $\tilde{\phi}$). The area-weighted grid-mean vertical velocity is $\overline{w} = \sum_i \hat{a}^i \hat{w}_o^i + \sum_j \check{a}^j \check{w}_o^j + \tilde{a}\tilde{w}_o$, where the overbar denotes a grid mean. We define relative mass fluxes $\hat{M}^i \equiv \rho \hat{a}^i \hat{w}^i$, $\check{M}^j \equiv \rho \check{a}^j \check{w}^j$, and $\tilde{M} \equiv \rho \tilde{a} \tilde{w}$ using relative vertical velocities $\hat{w}^i \equiv \hat{w}_o^i - \overline{w}$, $\check{w}^j \equiv \check{w}_o^j - \overline{w}$, and $\tilde{w} \equiv \tilde{w}_o - \overline{w}$, which satisfy $\sum_i \hat{M}^i + \sum_j \check{M}^j + \tilde{M} = 0$. Here ρ is the air density, and the anelastic approximation will be used. From now on, we will use a simplified notation without the indices i and j (unless they are apparently necessary), so that $\hat{x}$ and $\check{x}$ will denote $\hat{x}^i$ and $\check{x}^j$, respectively, for any variable x. Assuming both convective updrafts and downdrafts are mixed with the environmental air without direct mass exchange between convective updrafts and downdrafts, the mass conservation principle within an individual volume area can be formulated as

$$\frac{\partial \hat{a}}{\partial t} = -\overline{\mathbf{V}} \cdot \nabla \hat{a} - g \frac{\partial \hat{M}}{\partial p} + \frac{1}{\rho}(\hat{E} - \hat{D}), \tag{1}$$

$$\frac{\partial \check{a}}{\partial t} = -\overline{\mathbf{V}} \cdot \nabla \check{a} - g \frac{\partial \check{M}}{\partial p} + \frac{1}{\rho}(\check{E} - \check{D}), \quad \text{and} \tag{2}$$

$$\frac{\partial \tilde{a}}{\partial t} = -\overline{\mathbf{V}} \cdot \nabla \tilde{a} + g \frac{\partial}{\partial p} \sum_i \hat{M}^i + g \frac{\partial}{\partial p} \sum_j \check{M}^j - \frac{1}{\rho}\left[\sum_i (\hat{E}^i - \hat{D}^i) + \sum_j (\check{E}^j - \check{D}^j) \right], \tag{3}$$

where the pressure-coordinate $p \equiv p_s - p_r$ (p_s and p_r are the surface pressure and the pressure above the surface, respectively) is defined increasing upward, $-\overline{\mathbf{V}} \cdot \nabla \psi = -\overline{u}\partial\psi/\partial x - \overline{v}\partial\psi/\partial y - \overline{\omega}\partial\psi/\partial p$ is the grid-scale advection of scalar ψ by the grid-mean flow ($\overline{\omega} \equiv Dp/Dt$ is a grid-mean pressure-vertical velocity), and $(\hat{E}, \hat{D}, \check{E}, \check{D}) \geq 0$ are the convergence of mass flux from environment to updraft $\hat{E}$, from updraft to environment $\hat{D}$, from environment to downdraft $\check{E}$, and from downdraft to environment $\check{D}$. The conservation principle of scalar content within an individual volume area in each layer can be written as follows:

$$\frac{\partial}{\partial t}(\hat{a}\hat{\phi}) = -\overline{\mathbf{V}} \cdot \nabla(\hat{a}\hat{\phi}) - g \frac{\partial}{\partial p}(\hat{M}\hat{\phi}) + \frac{1}{\rho}(\hat{E}\tilde{\phi}_u - \hat{D}\hat{\phi}_*) + \hat{a}\left[\left(\frac{\partial \hat{\phi}}{\partial t} \right)_s + \left(\frac{\partial \hat{\phi}}{\partial t} \right)_c \right], \tag{4}$$

$$\frac{\partial}{\partial t}(\check{a}\check{\phi}) = -\overline{\mathbf{V}} \cdot \nabla(\check{a}\check{\phi}) - g \frac{\partial}{\partial p}(\check{M}\check{\phi}) + \frac{1}{\rho}(\check{E}\tilde{\phi}_d - \check{D}\check{\phi}_*) + \check{a}\left[\left(\frac{\partial \check{\phi}}{\partial t} \right)_s + \left(\frac{\partial \check{\phi}}{\partial t} \right)_c \right], \quad \text{and} \tag{5}$$

$$\frac{\partial}{\partial t}(\tilde{a}\tilde{\phi}) = -\overline{\mathbf{V}} \cdot \nabla(\tilde{a}\tilde{\phi}) + g\left[\frac{\partial}{\partial p}\left(\tilde{\phi} \sum_i \hat{M}^i \right) + \frac{\partial}{\partial p}\left(\tilde{\phi} \sum_j \check{M}^j \right) \right] - \frac{1}{\rho}\left[\sum_i (\hat{E}^i \tilde{\phi}_u - \hat{D}^i \hat{\phi}_*^i) + \sum_j (\check{E}^j \tilde{\phi}_d - \check{D}^j \check{\phi}_*^j) \right] + \tilde{a}\left(\frac{\partial \tilde{\phi}}{\partial t} \right)_s - \sum_i \hat{a}^i \left(\frac{\partial \hat{\phi}^i}{\partial t} \right)_c - \sum_j \check{a}^j \left(\frac{\partial \check{\phi}^j}{\partial t} \right)_c, \tag{6}$$

where $\hat{\phi}^i_*$ and $\check{\phi}^j_*$ are the detrained scalars from each convective updraft and downdraft, respectively; $\tilde{\phi}_u$ and $\tilde{\phi}_d$ are the environmental scalars involved in the mixing with convective updraft and downdraft (so-called mixing environmental scalars from now on); $(\partial\hat{\phi}^i/\partial t)_s$, $(\partial\check{\phi}^j/\partial t)_s$, and $(\partial\tilde{\phi}/\partial t)_s$ are sources in each volume area; while $(\partial\hat{\phi}^i/\partial t)_c$ and $(\partial\check{\phi}^j/\partial t)_c$ are direct conversion terms from environment to convective updrafts and downdrafts, respectively, without mass exchange. The blocking of the environmental horizontal wind by convective plumes corresponds to $(\partial\hat{\phi}^i/\partial t)_c$ and $(\partial\check{\phi}^j/\partial t)_c$ for $\phi = u, v$. The asterisk denotes the scalar properties of convective plumes involved in the mixing, which can differ from the mean properties of the convective updraft and downdraft owing to the possible existence of inhomogeneity in each volume area. By inserting the mass conservation equations [Eqs. (1)–(3)] into the conservation equations of scalar content [Eqs. (4)–(6)], we can derive the following scalar conservation equations:

$$\hat{a}\frac{\partial\hat{\phi}}{\partial t} = -\hat{a}\overline{\mathbf{V}}\cdot\nabla\hat{\phi} - g\hat{M}\frac{\partial\hat{\phi}}{\partial p} - \frac{1}{\rho}[\hat{E}(\hat{\phi}-\tilde{\phi}_u) + \hat{D}(\hat{\phi}_*-\hat{\phi})] + \hat{a}\left[\left(\frac{\partial\hat{\phi}}{\partial t}\right)_s + \left(\frac{\partial\hat{\phi}}{\partial t}\right)_c\right], \tag{7}$$

$$\check{a}\frac{\partial\check{\phi}}{\partial t} = -\check{a}\overline{\mathbf{V}}\cdot\nabla\check{\phi} - g\check{M}\frac{\partial\check{\phi}}{\partial p} - \frac{1}{\rho}[\check{E}(\check{\phi}-\tilde{\phi}_d) + \check{D}(\check{\phi}_*-\check{\phi})] + \check{a}\left[\left(\frac{\partial\check{\phi}}{\partial t}\right)_s + \left(\frac{\partial\check{\phi}}{\partial t}\right)_c\right], \quad \text{and} \tag{8}$$

$$\tilde{a}\frac{\partial\tilde{\phi}}{\partial t} = -\tilde{a}\overline{\mathbf{V}}\cdot\nabla\tilde{\phi} + g\left(\sum_i\hat{M}^i + \sum_j\check{M}^j\right)\frac{\partial\tilde{\phi}}{\partial p} - \frac{1}{\rho}\left\{\sum_i[\hat{D}^i(\tilde{\phi}-\hat{\phi}^i_*) + \hat{E}^i(\tilde{\phi}_u-\tilde{\phi})] + \sum_j[\check{D}^j(\tilde{\phi}-\check{\phi}^j_*) + \check{E}^j(\tilde{\phi}_d-\tilde{\phi})]\right\} + \tilde{a}\left(\frac{\partial\tilde{\phi}}{\partial t}\right)_s - \sum_i\hat{a}^i\left(\frac{\partial\hat{\phi}^i}{\partial t}\right)_c - \sum_j\check{a}^j\left(\frac{\partial\check{\phi}^j}{\partial t}\right)_c. \tag{9}$$

For simplicity, we assume that the plume properties are invariant to the Lagrangian displacement by the grid-mean flow (i.e., $D\psi/Dt \equiv \partial\psi/\partial t + \overline{\mathbf{V}}\cdot\nabla\psi = 0$, where $\psi = \hat{a}, \check{a}, \hat{\phi}, \check{\phi}$); that is, we use a quasi-conserved plume approximation. If the advection tendency of the plume properties by the grid-mean flow is assumed to be negligible (e.g., $\overline{\mathbf{V}}\cdot\nabla\psi \approx 0$ when G is very large), our quasi-conserved plume approximation is reduced to the conventional quasi-steady plume approximation of $\partial\psi/\partial t = 0$. With this approximation, Eqs. (1), (2), (7), and (8) are simplified to

$$\frac{1}{\hat{M}}\frac{\partial\hat{M}}{\partial p} = \hat{\epsilon} - \hat{\delta}, \tag{10}$$

$$\frac{1}{\check{M}}\frac{\partial\check{M}}{\partial p} = \check{\epsilon} - \check{\delta}, \tag{11}$$

$$\frac{\partial\hat{\phi}}{\partial p} = -\hat{\epsilon}(\hat{\phi}-\tilde{\phi}_u) - \hat{\delta}(\hat{\phi}_*-\hat{\phi}) + \hat{S}_\phi + \hat{C}_\phi, \quad \text{and} \tag{12}$$

$$\frac{\partial\check{\phi}}{\partial p} = -\check{\epsilon}(\check{\phi}-\tilde{\phi}_d) - \check{\delta}(\check{\phi}_*-\check{\phi}) + \check{S}_\phi + \check{C}_\phi, \tag{13}$$

where $\hat{\epsilon} \equiv \hat{E}/(\rho g\hat{M})$ and $\hat{\delta} \equiv \hat{D}/(\rho g\hat{M})$ are fractional entrainment and detrainment rates of the convective updraft plumes; $\check{\epsilon} \equiv \check{E}/(\rho g\check{M})$ and $\check{\delta} \equiv \check{D}/(\rho g\check{M})$ are fractional entrainment and detrainment rates of convective downdraft plumes;

$$\hat{S}_\phi \equiv \left(\frac{\hat{a}}{g\hat{M}}\right)\left(\frac{\partial\hat{\phi}}{\partial t}\right)_s = \left(\frac{\partial\hat{\phi}}{\partial p}\right)_s,$$

$$\check{S}_\phi \equiv \left(\frac{\check{a}}{g\check{M}}\right)\left(\frac{\partial\check{\phi}}{\partial t}\right)_s = \left(\frac{\partial\check{\phi}}{\partial p}\right)_s \tag{14}$$

are sources within each convective plume per incremental vertical displacement; and

$$\hat{C}_\phi \equiv \left(\frac{\hat{a}}{g\hat{M}}\right)\left(\frac{\partial\hat{\phi}}{\partial t}\right)_c = \left(\frac{\partial\hat{\phi}}{\partial p}\right)_c,$$

$$\check{C}_\phi \equiv \left(\frac{\check{a}}{g\check{M}}\right)\left(\frac{\partial\check{\phi}}{\partial t}\right)_c = \left(\frac{\partial\check{\phi}}{\partial p}\right)_c \tag{15}$$

are the incremental changes of the scalars within each convective plume due to direct conversion from environment to individual plumes without mass exchange. The goal of a convection scheme is to compute the grid-mean tendency due to subgrid vertical transport by nonlocal asymmetric turbulent eddies. From Eq. (9), the convective tendency equation of grid-mean scalars expressed in terms of subsidence detrainment becomes

$$\begin{aligned}\frac{\partial\overline{\phi}}{\partial t}+\overline{\mathbf{V}}\cdot\nabla\overline{\phi}&=\tilde{a}\left(\frac{\partial\tilde{\phi}}{\partial t}+\overline{\mathbf{V}}\cdot\nabla\tilde{\phi}\right)\\&=g\left(\sum_i\hat{M}^i+\sum_j\check{M}^j\right)\frac{\partial\tilde{\phi}}{\partial p}+\left(\frac{g}{\Delta p}\right)\left[\sum_i\Delta\hat{M}^i_\delta(\hat{\phi}^i_*-\tilde{\phi})+\sum_j\Delta\check{M}^j_\delta(\check{\phi}^j_*-\tilde{\phi})\right]\\&\quad-\left(\frac{g}{\Delta p}\right)\left[\sum_i\Delta\hat{M}^i_\epsilon(\tilde{\phi}_u-\tilde{\phi})+\sum_j\Delta\check{M}^j_\epsilon(\tilde{\phi}_d-\tilde{\phi})\right]-g\left(\sum_i\hat{M}^i\hat{C}^i_\phi+\sum_j\check{M}^j\check{C}^j_\phi\right)+\tilde{a}\left(\frac{\partial\tilde{\phi}}{\partial t}\right)_s,\end{aligned}\tag{16}$$

where $\Delta\hat{M}_\epsilon=\hat{\epsilon}\hat{M}\Delta p\ge 0$ and $\Delta\check{M}_\epsilon=\check{\epsilon}\check{M}\Delta p\ge 0$ are the entrained masses from environment to each convective updraft and downdraft per unit time per unit area, respectively, and $\Delta\hat{M}_\delta=\hat{\delta}\hat{M}\Delta p\ge 0$ and $\Delta\check{M}_\delta=\check{\delta}\check{M}\Delta p\ge 0$ are the detrained masses from each convective plume to the environment in the model layer with a pressure thickness $\Delta p>0$. Using Eqs. (10)–(13), Eq. (16) can also be written in the following convergence-source form:

$$\begin{aligned}\frac{\partial\overline{\phi}}{\partial t}+\overline{\mathbf{V}}\cdot\nabla\overline{\phi}&=-g\frac{\partial}{\partial p}\left[\sum_i\hat{M}^i(\hat{\phi}^i-\tilde{\phi})+\sum_j\check{M}^j(\check{\phi}^j-\tilde{\phi})\right]\\&\quad+g\left(\sum_i\hat{M}^i\hat{S}^i_\phi+\sum_j\check{M}^j\check{S}^j_\phi\right)+\tilde{a}\left(\frac{\partial\tilde{\phi}}{\partial t}\right)_s,\end{aligned}\tag{17}$$

where the rhs denotes the grid-mean tendencies by various physical processes. The grid-mean tendencies by nonconvective physical processes can be treated as parts of the environmental source term on the rhs. With appropriate sources, UNICON uses Eq. (17) to compute the grid-mean convective tendencies of nonconservative scalars $\phi=q_l, q_i, n_l$, and n_i (where n_l and n_i are grid-mean number concentrations of cloud liquid droplets and ice crystals), as well as $\phi=q_t$, θ_c, u, v, and ξ, which are conserved scalars during adiabatic vertical displacement and associated phase changes [$q_t\equiv q_v+q_l+q_i$ is total specific humidity; $\theta_c\equiv\theta-(L_v/C_p/\pi)\times q_l-(L_s/C_p/\pi)\times q_i$ is condensate potential temperature; L_v and L_s are the latent heats of vaporization and sublimation, respectively; C_p is a specific heat at constant pressure; $\pi\equiv(p_r/p_o)^{R_d/C_p}$ is an Exner function with $p_o=1000$ hPa and R_d is a gas constant of dry air; and ξ is the mass and number concentration of aerosols and chemical species]. The grid-mean convective tendency of q_v is derived from the grid-mean convective tendencies of q_t and q_l, q_i.

Before discussing the detailed parameterization of unknown terms, the fundamental assumptions on which our simplified governing equations [Eqs. (10)–(17)] are based will be explained: 1) the parameterized convection does not induce grid-mean vertical motion (i.e., $\sum_i\hat{M}^i+\sum_j\check{M}^j+\tilde{M}=0$), 2) convective plumes are not horizontally overlapped (i.e., $\sum_i\hat{a}^i+\sum_j\check{a}^j+\tilde{a}=1$), and 3) convective plumes are quasi conserved, and so diagnostic (i.e., $D\psi/Dt\equiv\partial\psi/\partial t+\overline{\mathbf{V}}\cdot\nabla\psi=0$, where $\psi=\hat{a}$, $\check{a}$, $\hat{\phi}$, $\check{\phi}$).

The first assumption dictates the fundamental principle of convective parameterization in any gridded atmospheric model: the convection scheme parameterizes relative subgrid vertical transport with respect to the grid-mean vertical flow simulated by the grid-scale advection scheme. This means that the observed convection system and associated vertical transport are completely simulated through the combination of mutually exclusive but interactive, grid-scale advection and subgrid convection schemes. In order to explain how the partitioning of the observed convection system into convection–advection processes occurs in the gridded model, we exemplify in Fig. 2 several possible configurations of the relative sizes and the locations of $G=\Delta x\Delta y$, $\pi\hat{R}^2_{\rm obs}$, and $\pi R^2_{\rm cs,obs}$, where $\hat{R}_{\rm obs}$ and $R_{\rm cs,obs}$ are the radii of the observed cumulus and compensating subsidence, respectively, and $\hat{R}_{\rm obs}\ll R_{\rm cs,obs}$. If $\pi\hat{R}^2_{\rm obs}\ll G\approx\pi R^2_{\rm cs,obs}$ (Fig. 2a when the so-called spatial quasi-equilibrium assumption is valid), the grid-scale advection scheme does not simulate the observed convection but the subgrid convection scheme simulates the entire observed convection system. If $G\to\pi\hat{R}^2_{\rm obs}$ (Fig. 2b), the grid-scale advection scheme simulates most of the observed convection system (i.e., $\overline{w}\to\hat{w}_{\rm obs}$) and the subgrid convection scheme simulates the remaining relative subgrid transport with respect to $\overline{w}$ within G. Except in the limiting cases when $G<\pi\hat{R}^2_{\rm obs}$ is entirely located within the homogeneous observed cumulus (Fig. 2c) or compensating subsiding area (Fig. 2f), the subgrid convection scheme still contributes to the vertical transport

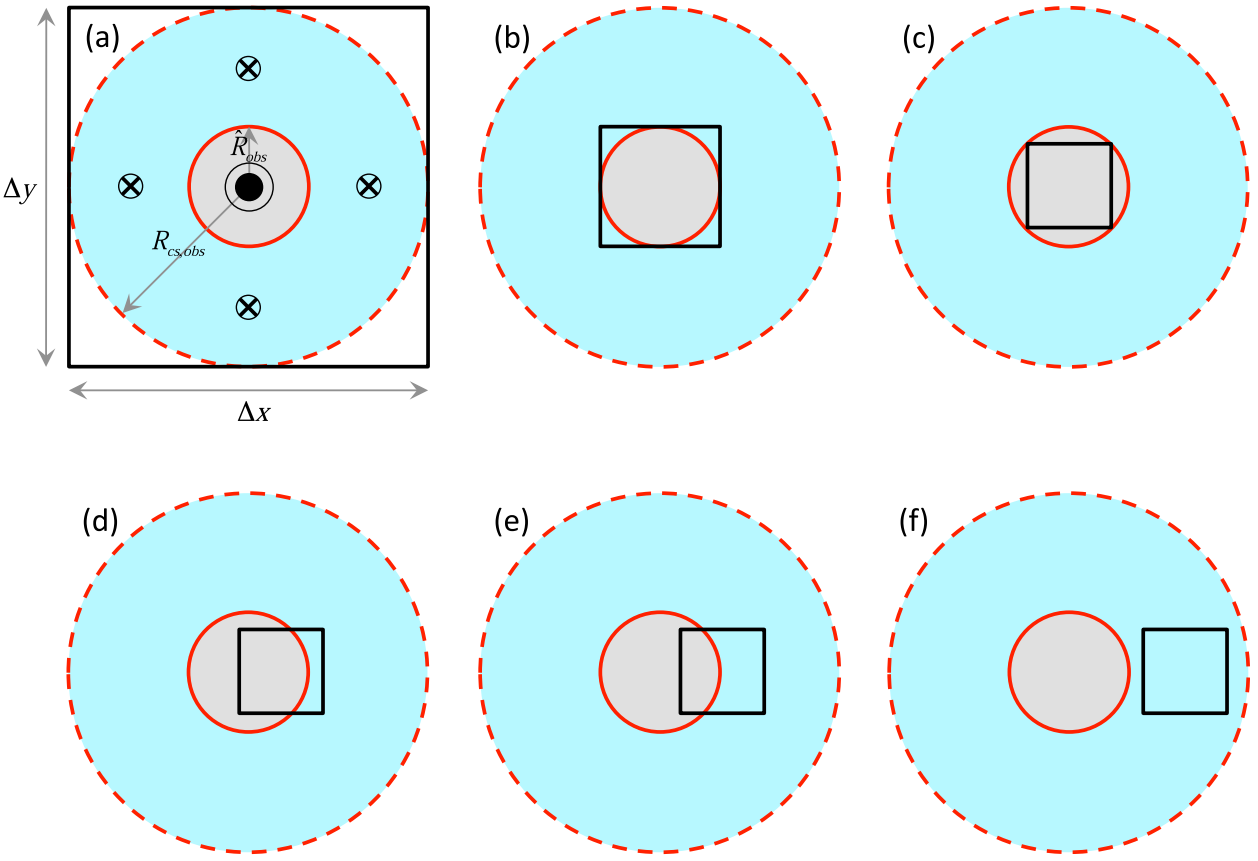

FIG. 2. The relative configurations of an observed convective updraft with rising motion (⊙) within the radius of $\hat{R}_{\rm obs}$, compensating subsidence with subsiding motion (⊗) between $\hat{R}_{\rm obs}$ and $R_{\rm cs,obs}$ induced by an observed convective updraft, and the GCM grid with a horizontal size of $G \equiv \Delta x \Delta y$. In the case of a quasi-conserved diagnostic plume model with $\sum_i \hat{a}^i \le \hat{A}_{\max} \ll 1$, (a) $\pi \hat{R}^2_{\rm obs} \ll G \approx \pi R^2_{\rm cs,obs}$, where all the observed convection phenomena are subgrid processes (in this case, many cumuli can exist within G, but for simplicity, only one cumulus is shown, by noting that similar interpretation can be made for the other cumuli); (b) $G \to \pi \hat{R}^2_{\rm obs}$ and $\overline{w} \to \hat{w}_{\rm obs}$, where most of the observed convective updraft is simulated by the grid-scale advection scheme, and UNICON simulates the remaining relative subgrid vertical transport with respect to the grid-mean flow; (c) $G < \pi \hat{R}^2_{\rm obs}$ and $\overline{w} = \hat{w}_{\rm obs}$, where the grid-scale advection scheme entirely simulates the observed convective updraft, and UNICON becomes inactive due to zero buoyancy of the convective updraft; (d),(e) $G < \pi \hat{R}^2_{\rm obs}$ and $w_{\rm cs,obs} < \overline{w} < \hat{w}_{\rm obs}$, where UNICON still performs subgrid vertical transport even for this small G; (f) $G < \pi \hat{R}^2_{\rm obs}$ and $\overline{w} = w_{\rm cs,obs}$, where the observed compensating subsidence is entirely simulated by the grid-scale advection scheme, and UNICON is likely to be inactive due to strong environmental stratification within G. Except for the case of (a), the analogy between the observed convective updraft and the UNICON-simulated subgrid convective updraft is broken. If a prognostic convection scheme is used, then $\sum_i \hat{a}^i \le 1$ [e.g., $\sum_i \hat{a}^i = 1$ for (c)] and the analogy between the observed convective updraft and the simulated subgrid convective updraft is always maintained. See sections 2a and 3 for details.

even in small $G < \pi \hat{R}^2_{\rm obs}$ (Figs. 2d,e); that is, similar to the PBL scheme, the subgrid convection scheme should be functional regardless of the size of G. This seamless partitioning of the observed convection system into convection–advection processes over a wide range of G is one of the key conditions required for the scale-adaptive GCMs. In section 3, we will discuss how UNICON handles this seamless partitioning within the framework of a diagnostic plume model.

The second assumption of horizontal nonoverlap is appropriate if the GCM integration time step Δt is much shorter than the life cycle of convection, so that UNICON depicts an instantaneous snap shot of convection. Within a long Δt [=1800 s for the Community Atmosphere Model, version 5 (CAM5; Park et al. 2014), with 30 vertical layers], however, the observed convective plumes can evolve, so that some of the precedent convective updraft area can be occupied by the subsequent convective downdraft within Δt, making the horizontal nonoverlap assumption inappropriate. Within the framework of conventional parameterization, it is practically impossible to track the evolution of complex overlap structures between convective updrafts and downdrafts during Δt. In order to bypass this dilemma, we will assume $\breve{a} \to 0$.

The third assumption of the quasi-conserved convective plumes substantially simplifies our governing equations. This assumption is equivalent to constructing diagnostic plume profiles at the beginning of the convection scheme, performing vertical transport through these plumes, and removing (not detraining) the plumes without adding to the grid-mean tendency at the end of the convection scheme. This diagnostic plume approximation, however, inevitably loses the memory of the plume properties between the model time steps, since the mean environmental profile—the only prognosed variable in typical diagnostic plume models—does not contain explicit information about the internal properties of the parameterized convective plumes. This lack of plume memory seems to be one reason that conventional diagnostic convection schemes fail to simulate the diurnal cycle of precipitation and the MJO (Park 2014). The naive way to carry the plume memory across Δt is to solve the prognostic equations for convective plumes [Eqs. (1)–(3) and (7)–(9)], which can, however, induce numerical instability in a GCM with a large Δt. Given the fact that the validity of the quasi-equilibrium assumption is highly questionable in small temporal and spatial domains, the approach adopted by UNICON is to carry additional plume memory through the prognostic cold pool and mesoscale organized flow forced by convective plumes and use that memory to reconstruct convective plumes at subsequent time steps, as will be detailed in sections 2d and 2e. This combined approach of diagnostic convective updraft and downdraft plumes, prognostic cold pool and mesoscale organized flows, and feedback between them will remedy the issue concerning lack of plume memory in typical diagnostic plume models. Finally, we note that owing to the diagnostic nature of the quasi-conserved plumes, there is no need to advect the plume properties. Thus, in the process-splitting CAM5 in which UNICON is operating on the mean input state updated by the proceeding grid-scale advection scheme ($\phi_{\rm adv}$; Park et al. 2014), it becomes $\phi_{\rm adv} = \tilde{\phi}$. However, if a prognostic plume model is used [e.g., Eqs. (1)–(3) and (7)–(9)], it will be $\phi_{\rm adv} = \overline{\phi} = \sum_i \hat{a}^i \hat{\phi}^i + \sum_j \check{a}^j \check{\phi}^j + \tilde{a}\tilde{\phi}$.

b. Convective updraft

1) Onset at the surface

We assume an individual updraft plume rises from the surface. The key idea to initialize thermodynamic properties of updraft plumes is to match the reconstructed surface flux by UNICON with the input surface flux given from a separate surface flux computation routine. At the surface, we assume w and any conservative scalar ϕ ($=q_t$, θ_c, u, v, ξ) follow a Gaussian distribution with a given covariance (i.e., input surface flux). Following Park et al. (2004), UNICON reconstructs the given covariance between w and ϕ using a common standardized variable α, defined as

$$\alpha = \frac{\hat{w}(\alpha) - \Delta w_\Omega}{\sigma_w} = \frac{\hat{\phi}(\alpha) - \Delta\phi_\Omega - \overline{\phi}_s}{\sigma_\phi}, \quad 0 \le \alpha < \infty, \tag{18}$$

where σ_w and σ_ϕ are the standard deviations of w and ϕ, $\overline{\phi}_s$ is the grid-mean value at the surface ($\hat{\alpha}$ is already defined as a relative vertical velocity), Δw_Ω and $\Delta\phi_\Omega$ are components associated with subgrid mesoscale organized flow within the PBL [Eqs. (73) and (74)], and $0 \le \Omega \le 1$ is a parameter measuring the degree of subgrid mesoscale convective organization [Eq. (72)] with $\Omega = 0$ (1) denoting nonorganized (maximally organized) state. Note that σ_ϕ can be either positive or negative depending on the sign of the input surface flux. Equation (18) implies that turbulent updraft eddies at the surface parameterized by UNICON are uniformly distributed over the range of $0 \le \alpha < \infty$. We assume that the area probability density function (PDF) $P_a(\alpha) \equiv da(\alpha)/d\alpha$ in the range $(\alpha, \alpha + d\alpha)$ at the surface follows the Gaussian distribution with a specified net convective updraft fractional area, $0 \le \hat{A}_s \le 0.5$,

$$P_a(\alpha) = 2\hat{A}_s \frac{1}{\sqrt{2\pi}} \exp\left(-\frac{\alpha^2}{2}\right), \tag{19}$$

where $\int_0^\infty P_a(\alpha)\, d\alpha = \hat{A}_s$. The corresponding mass flux PDF $P_M(\alpha) \equiv dM(\alpha)/d\alpha$ is

$$P_M(\alpha) = \overline{\rho}_s P_a(\alpha)(\sigma_w \alpha + \Delta w_\Omega), \tag{20}$$

and, similar to PB09, we parameterize

$$\sigma_w = k_w \sqrt{e_{\rm PBL}}, \tag{21}$$

where $e_{\rm PBL}$ is turbulent kinetic energy (TKE) averaged over the PBL obtained from a separate PBL scheme, and k_w is an anisotropic factor of nonorganized turbulence. In order to reduce the sensitivity to the vertical resolution, Eq. (21) uses $e_{\rm PBL}$, rather than the more conceptually consistent $e_{\rm sfc}$, TKE near the surface. We note that $e_{\rm sfc}$ is roughly similar to $e_{\rm PBL}$, at least for convective PBLs (Bretherton and Park 2009), and the test simulation with $e_{\rm sfc}$ produced a similar result to the simulation with $e_{\rm PBL}$. In CAM5, the PBL-top height is defined in a complex manner using the Richardson number and the merging criteria (Bretherton and Park 2009; Park et al. 2014). If turbulence is isotropic, $k_w = \sqrt{2/3} \approx 0.82$, but the atmospheric static stability near the surface is likely to modify k_w (Mellor and Yamada 1982; Galperin

et al. 1988). UNICON is developed to be applicable in the stable as well as convective regimes without discontinuity, so that we use e_{PBL} rather than w_* (convective velocity).

In order to complete the initialization of convective updraft plumes, we should derive σ_ϕ for each conservative scalar. Using Eqs. (18) and (19), the matching condition between the reconstructed surface flux by UNICON and a given surface flux by nonorganized turbulence is $(\overline{w'\phi'})_s|_{\Omega=0} = (1/\hat{A}_s)\int_0^\infty [\hat{w}(\alpha) - \Delta w_\Omega][\hat{\phi}(\alpha) - \Delta\phi_\Omega - \overline{\phi}_s]P_a(\alpha)\,d\alpha = \sigma_w\sigma_\phi$, which results in

$$\sigma_\phi = \frac{(\overline{w'\phi'})_s|_{\Omega=0}}{\sigma_w}. \tag{22}$$

Most GCMs provide convection schemes with surface fluxes of sensible heat, water vapor, horizontal momentum, and tracers. Since all GCMs compute the surface flux using a simple similarity theory (Monin and Obukhov 1954) without considering the contribution of subgrid mesoscale organized flow within the surface layer, the input surface flux given to the convection scheme in GCMs is $(\overline{w'\phi'})_s|_{\Omega=0}$. Because the similarity theory implicitly assumes a constant flux layer from the surface to the top of the surface layer (which is assumed to be the midpoint of the lowest model layer in the numerical models), Eq. (22) is valid so long as the origination level of convective updraft plumes (which is set to the surface in UNICON) is below the midpoint of the lowest model layer. The derivation of Eq. (22) is also based on the implicit assumption of the surface layer similarity theory that surface flux generated by turbulent updraft eddies is the same as the one generated by turbulent downdraft eddies.

UNICON parameterizes the fractional mixing rate $\hat{\epsilon}_o$ between convective updrafts and the environment (or detrained air) as an inverse function of updraft plume radius $\hat{R}$ [Eq. (31)], whose vertical profile and time evolution are internally computed once the values at the nonorganized and maximally organized states are given at the surface [Eqs. (30), (76), and (77)]. Similar to the other scalars, the radius of individual convective updrafts at the surface is parameterized as a linearly increasing function of α,

$$\hat{R}(\alpha) = R_o + \sigma_R\alpha, \tag{23}$$

where R_o is the intercept plume radius at $\alpha = 0$ and σ_R is the standard deviation of updraft plume radius at the surface. The above equation is applied for updraft eddies [i.e., $0 \le \alpha < \infty$ and $\hat{R}(\alpha) \ge R_o$]. The number density PDF of convective updraft plumes $P_n(\alpha)$ within $(\alpha, \alpha + d\alpha)$ becomes

$$P_n(\alpha) = \frac{P_a(\alpha)}{\pi\hat{R}^2(\alpha)}. \tag{24}$$

The fractional area $\hat{a}(\alpha)$ and the mass flux $\hat{M}(\alpha)$ of the convective updraft plume in the range $(\alpha, \alpha + \Delta\alpha)$ are $\hat{a}(\alpha) = P_a(\alpha)\Delta\alpha$ and $\hat{M}(\alpha) = P_M(\alpha)\Delta\alpha$. For numerical computation, we impose an upper limit of $\alpha_{\max} = 2$ to α with $\Delta\alpha = \alpha_{\max}/\hat{n}_s$, where $\hat{n}_s$ is the number of convective updraft segments at the surface externally specified. Individual updraft segments for $\alpha = \Delta\alpha \times (i - 0.5) \le \alpha_{\max}$ with $i = 1, 2, \ldots, \hat{n}_s$ are launched with $\hat{\phi}(\alpha)$, $\hat{w}(\alpha)$, $\hat{M}(\alpha)$, $\hat{a}(\alpha)$, and $\hat{R}(\alpha)$ (see Fig. 3). Note that $\hat{\phi}^i$ in the governing equations in the previous section is $\hat{\phi}^i = \hat{\phi}(\alpha)$ at the surface (and similarly for $\hat{w}$, $\hat{M}$, $\hat{a}$, $\hat{R}$).

2) Vertical evolution: Analytic solutions

The vertical evolution of the mass flux and the scalars of individual convective updrafts are determined by Eqs. (10) and (12). By assuming the internal homogeneity of an individual updraft plume (i.e., $\hat{\phi}_* = \hat{\phi}$); a linear profile of mixing environmental scalars; and height-independent $\hat{\epsilon}$, $\hat{\delta}$, and $\hat{C}_\phi$ within each layer, analytical solutions of Eqs. (10) and (12) without $\hat{S}_\phi$ become

$$\hat{M}^{\mathrm{top}} = \hat{M}^{\mathrm{bot}}\exp[(\hat{\epsilon} - \hat{\delta})\Delta p] \quad \text{and} \tag{25}$$

$$\hat{\phi}^{\mathrm{top}} = \left[\tilde{\phi}_u^{\mathrm{top}} - \left(\frac{\tilde{\gamma}_u - \hat{C}_\phi}{\hat{\epsilon}}\right)\right] - \left[\tilde{\phi}_u^{\mathrm{bot}} - \left(\frac{\tilde{\gamma}_u - \hat{C}_\phi}{\hat{\epsilon}}\right) - \hat{\phi}^{\mathrm{bot}}\right]\exp(-\hat{\epsilon}\Delta p), \tag{26}$$

where $\Delta p > 0$ is the updraft vertical displacement in each layer, superscripts "bot" and "top" denote the values at the base and top interfaces, $\tilde{\phi}_u$ are mixing environmental scalars for convective updrafts, and $\tilde{\gamma}_u \equiv \Delta\tilde{\phi}_u/\Delta p$ is the vertical slope of mixing environmental scalars. Equation (26) is applied for individual conservative scalars $\phi = q_t, \theta_c$, u, v, and ξ. If $\phi = q_t$ or θ_c, then $\hat{C}_\phi = 0$ and the corresponding sources $\hat{S}_\phi$ associated with the production of convective precipitation are discretely added at the top interface after solving Eq. (26). If $\phi = \xi$, $\hat{C}_\phi = 0$ and $\hat{S}_\phi \le 0$ since aerosols and chemical species are scavenged out by convective precipitation within convective updrafts [Eq. (39)]. If $\phi = u$ or v, $\hat{C}_\phi \ne 0$ but $\hat{S}_\phi = 0$. The updraft values of $\phi = q_v, q_l, q_i$ at the top interface are computed from the updated $\phi = q_t, \theta_c$ assuming that an individual convective updraft is internally homogeneous. The ice fraction among the cloud condensate is simply set to be a ramping function of the updraft temperature between 233 and 263 K.

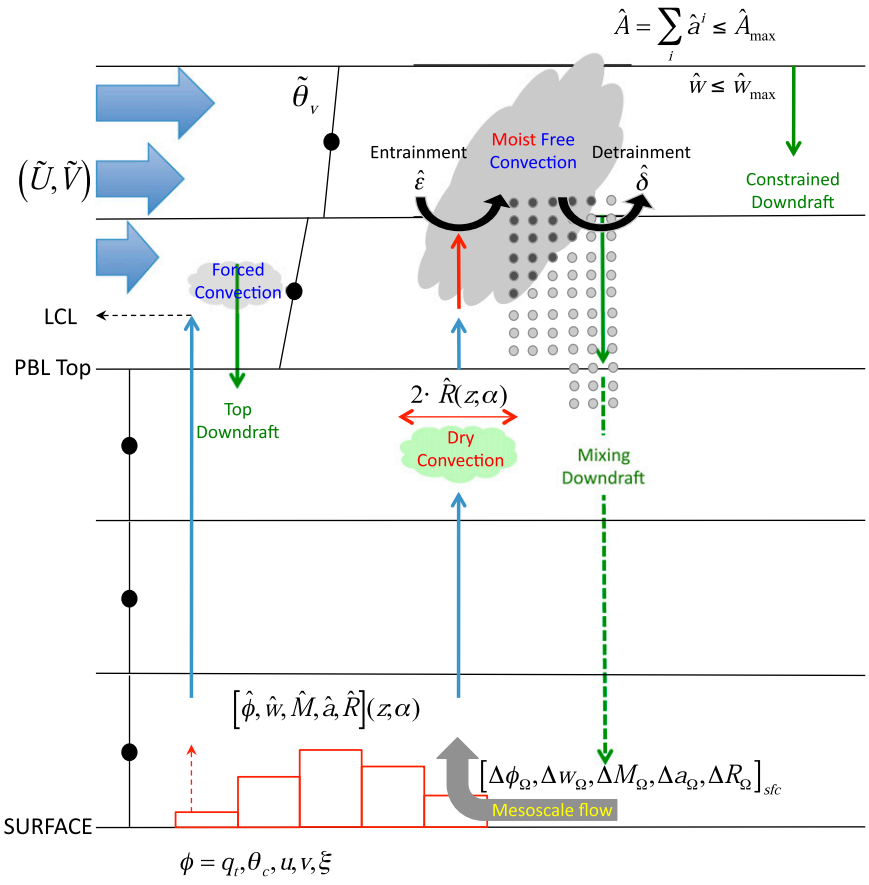

FIG. 3. Various parameterized physical processes within UNICON for given vertical profiles of virtual potential temperature $\tilde{\theta}_v$ and a horizontal wind vector $(\tilde{U}, \tilde{V})$ in the environment. A set of updraft plumes rising from the surface with initial thermodynamic $[\hat{\phi}(\alpha), \hat{w}(\alpha), \hat{M}(\alpha)]$ and macrophysical properties $[\hat{a}(\alpha), \hat{R}(\alpha)]$ entrain mixing environmental air and detrain internal air at the rates of $(\hat{\epsilon}, \hat{\delta}) \propto 1/\hat{R}$, respectively. In most cases, source updraft plumes are unsaturated at the surface but eventually become saturated at the LCL. At the LCL, some plumes are negatively buoyant and not strong enough to reach to the LFC; they sink down to the neutral buoyancy layer and are detrained into the environment. This forced convection is parameterized by the top downdraft. Some plumes grow over the LFC—free convection—and produce convective precipitation. Depending on the vertical tilting of an updraft plume controlled by $(\tilde{U}, \tilde{V})$, convective precipitation may fall into a saturated updraft (in which case no evaporation occurs) or into an unsaturated environment (in which case evaporation occurs). Some negatively buoyant mixtures generated during the mixing are converted into mixing downdrafts, which are cooled by evaporation of convective precipitation and penetrate into the PBL, generating a cold pool and mesoscale organized flow within the PBL. The properties of source updraft at the surface and mixing environmental air within and above the PBL are additionally modified by the mesoscale perturbation $(\Delta\phi_\Omega, \Delta w_\Omega, \Delta M_\Omega, \Delta a_\Omega, \Delta R_\Omega)$. If the net updraft fractional area $\hat{A}$ is larger than $\hat{A}_{\max}$ or $\hat{w} > \hat{w}_{\max}$ at each model interface, the excessive updraft mass fluxes are detrained, forming the constrained downdraft. See the text for details.

UNICON also computes the vertical evolution of updraft vertical velocity. During vertical displacement, the vertical velocity of an updraft plume can be changed by buoyancy, entrainment drag, detrainment thrust, and vertical perturbation pressure gradient force (PGF). Following the work of Simpson and Wiggert (1969), the vertical perturbation PGF is partitioned into buoyancy and inertial (or centripetal) forces. Then, the steady-state vertical velocity equation of a convective updraft becomes

$$\frac{1}{2}\frac{\partial \hat{w}^2}{\partial p} = [1 - v_1(\hat{R})]\frac{\hat{B}}{\rho g} - \left(\hat{\epsilon} + \frac{v_2}{\rho g \hat{R}} - c\hat{\delta}\right)\hat{w}^2$$

$$= a(\hat{R})\frac{\hat{B}}{\rho g} - (b\hat{\epsilon} - c\hat{\delta})\hat{w}^2, \qquad (27)$$

where $\hat{B} \equiv g(1-\hat{\rho}/\overline{\rho}) = (g/\overline{\theta}_v)(1-\hat{a})(\hat{\theta}_v - \tilde{\theta}_v^+)$ is the updraft buoyancy with $\tilde{\theta}_v^+ = [\tilde{a}\tilde{\theta}_v + \sum_{i\neq i_c}(\hat{a}^i\hat{\theta}_v^i)]/(1-\hat{a}^{i_c})$ (i_c denoting the current updraft index being considered; i.e., $\hat{a} = \hat{a}^{i_c}$ and $\tilde{\theta}_v^+ = \tilde{\theta}_v$ if only a single updraft exists in the current layer), and the two terms with v_1 and v_2 are the partitioning of vertical perturbation PGF into buoyancy and inertial drag. Since $\hat{B}$ is defined as the anomaly with respect to the grid-mean value within each grid layer, $\hat{w}$ is not total but relative vertical velocity. Accordingly, $\hat{R}$ in the above equation should be understood as the subgrid plume radius with a certain relative vertical velocity. Equation (27) implicitly assumes that the work of Simpson and Wiggert (1969) based on the total vertical velocity and the observed plume radius is also valid with the relative vertical velocity and the subgrid plume radius. The nondimensional coefficient $a(\hat{R}) = 1 - v_1(\hat{R})$ is the buoyancy coefficient, $b = 1 + v_2/[a_1(1+a_2E)\chi_c^2]$ [here, χ_c is a critical mixing fraction computed in Eq. (B2)] is the entrainment drag coefficient obtained by assuming that the entrainment rate $\hat{\epsilon}$ is proportional to $\hat{R}^{-1}$ [see Eqs. (31) and (33) with $p = 1$ in Eq. (35)], and c is the detrainment thrust coefficient. If the vertical velocity of the detrained air is identical to the vertical velocity of the convective updraft, $c = 0$. However, if the detrained air has a vertical velocity smaller than the updraft, $c > 0$ and a thrust will be provided to the remaining convective updraft. By assuming that $a(\hat{R})$, b, c, $\hat{\epsilon}$, $\hat{\delta}$, and ρ are height-independent constants within each grid layer, the analytical solution of Eq. (27) becomes

$$(\hat{w}^{\text{top}})^2 = (\hat{w}^{\text{bot}})^2 X + \left[\frac{a(\hat{R})}{\rho g(b\hat{\epsilon} - c\hat{\delta})}\right] \times \left\{\hat{\gamma}_B \Delta p + (1-X)\left[\hat{B}^{\text{bot}} - \frac{\hat{\gamma}_B}{2(b\hat{\epsilon} - c\hat{\delta})}\right]\right\}, \tag{28}$$

where $X \equiv \exp[-2(b\hat{\epsilon} - c\hat{\delta})\Delta p]$, $\hat{B}^{\text{bot}}$ is the updraft buoyancy at the bottom interface, and $\hat{\gamma}_B \equiv (\hat{B}^{\text{top}} - \hat{B}^{\text{bot}})/\Delta p$ is a linear slope of updraft buoyancy in each layer. We set $a(\hat{R})$ as a gradually decreasing function of $\hat{R}$ from 1 (when $\hat{R} = 0$) down to ⅓ (when $\hat{R} = \infty$):

$$a(\hat{R}) = \frac{1}{3}\left[1 + 2\exp\left(-\frac{\hat{R}}{R_a}\right)\right], \tag{29}$$

where R_a is an e-folding radius at which $a(R_a) = 0.58$. This formula comes from the fact that a plume with a large radius experiences stronger aerodynamic resistance during upward motion.

The fractional area $\hat{a}$ of an individual convective updraft plume is diagnosed from $\hat{M}$ and $\hat{w}$ using $\rho\hat{a} = \hat{M}/\hat{w}$. From the diagnosed $\hat{a}$, we compute $\hat{R}(z)$ at each level using

$$\hat{R}(z) = \left[\frac{\hat{a}(z)}{\pi P_n(\alpha)\Delta\alpha}\right]^{1/2}, \tag{30}$$

whenever an updraft plume reaches that model interface. Here, $P_n(\alpha)$ is a number density PDF defined at the surface [Eq. (24)].

3) Fractional mixing rate $\hat{\epsilon}_o$

Following Bretherton et al. (2004, hereafter BMG04) and PB09, UNICON assumes that a certain amount of updraft air ($\hat{\epsilon}_o\hat{M}\Delta p$) is mixed with the same amount of environmental air during vertical displacement $\Delta p > 0$. From the fractional mixing rate $\hat{\epsilon}_o$, UNICON computes the fractional entrainment ($\hat{\epsilon}$) and detrainment ($\hat{\delta}$) rates using the buoyancy sorting. Parameterization of $\hat{\epsilon}_o$ (or $\hat{\epsilon}$ and $\hat{\delta}$) is the most important, but uncertain, part of a convection scheme. The laboratory and observational studies in the 1960s found that $\hat{\epsilon}$ of a single updraft plume is inversely proportional to $\hat{R}$, with a proportional coefficient of around 0.2, regardless of whether the updraft plume is saturated (Saunders 1961; Turner 1962; Simpson et al. 1965). By assuming that $\hat{R}$ does not change much with height, this finding was used in many convection schemes (Arakawa and Schubert 1974; Tiedtke 1989; Kain and Fritsch 1990). However, subsequent studies using observations, large-eddy simulations (LESs) and cloud-resolving models (CRMs) have shown that $\hat{\epsilon}$ and $\hat{\delta}$ vary substantially with height. Consequently, many formulations have been proposed to parameterize $\hat{\epsilon}$ and $\hat{\delta}$, using factors other than the constant $\hat{R}$, such as the geometric height, updraft buoyancy, updraft vertical velocity, and the relative humidity of the environment (Gregory 2001; Neggers et al. 2002; Bechtold et al. 2008; PB09; de Rooy and Siebesma 2010; Stirling and Stratton 2012; Dawe and Austin 2013) for different cumulus types (e.g., shallow or deep cumulus, a single plume or an ensemble of multiple plumes). However, none of these are satisfactory and the underlying physics of such proposed formulations are unclear.

Given the lack of general consensus, UNICON uses the findings from the 1960s to parameterize $\hat{\epsilon}_o$. However, $\hat{R}$ is allowed to change with height and time, and as detailed here, the evaporative-cooling-driven entrainment mixing at the cumulus top is included. Following Kain and Fritsch (1990) and PB09, UNICON uses a buoyancy sorting to compute $\hat{\epsilon} = \hat{\epsilon}_o\chi_c^2$ [see Eq. (33) with $p = 1$ in Eq. (35)] where $0 \le \chi_c \le 1$ is a critical mixing fraction.

If a positively buoyant unsaturated updraft plume is mixed with unsaturated environmental air, $\chi_c = 1$ and so $\hat{\epsilon} = \hat{\epsilon}_o$. If an updraft plume contains condensate, however, χ_c can vary between 0 and 1 depending on the amount of updraft condensate, updraft buoyancy and vertical velocity, and environmental relative humidity, so that $\hat{\epsilon} \le \hat{\epsilon}_o$. This implies that in order to be consistent with the observed proportional coefficient of around 0.2 between $\hat{\epsilon}$ and $\hat{R}^{-1}$, $\hat{\epsilon}_o$ of a saturated plume should be larger than $\hat{\epsilon}_o$ of an unsaturated plume. Then, why is $\hat{\epsilon}_{o,\text{sat}} \ge \hat{\epsilon}_{o,\text{dry}}$? If unsaturated environmental air at the cumulus top is mixed with saturated updraft air containing condensate, evaporative cooling occurs during the mixing process, which pulls the mixture down into the cumulus updraft plume and triggers additional mixing to satisfy the mass conservation principle. This effect of evaporative cooling at the cumulus top and enhanced downward mixing has been noted by Squires (1958) and Emanuel (1981). In fact, similar evaporative enhancement of mixing occurs at the top of marine stratocumulus clouds, which is parameterized as a linear function of liquid water content (LWC) at the stratocumulus top in the CAM5 moist turbulence scheme (Bretherton and Park 2009).

Based on the above consideration, UNICON parameterizes $\hat{\epsilon}_0$ for an individual convective updraft as an inverse function of $\hat{R}$ with a proportional coefficient increasing with the updraft condensate amount and the degree of subsaturation of mixing environmental air:

$$\hat{\epsilon}_o(z) = \left[\frac{a_1}{\rho g \hat{R}(z)}\right](1 + a_2 E), \tag{31}$$

where $a_1 \approx 0.2$ is a dry mixing coefficient, a_2 is a moist mixing coefficient, and E is the evaporative enhancement factor defined as

$$E = \sqrt{(\hat{q}_l + \hat{q}_i)(1 - \widetilde{\text{RH}}_u)}, \tag{32}$$

where $\hat{q}_l + \hat{q}_i$ is in-cumulus condensate and $\widetilde{\text{RH}}_u$ is the relative humidity of mixing environmental air. Arguably, Eq. (32) is a crude attempt to quantify the degree of evaporative cooling during mixing that should be validated using observations in future. Bechtold et al. (2008) showed that imposing $\widetilde{\text{RH}}_u$ dependence on $\hat{\epsilon}$ improved simulations, although they did not provide physical justification on their approach. By considering enhanced entrainment mixing at the cumulus top driven by evaporative cooling, Eq. (31) collectively represents the mixing through both the lateral interface and the top of the convective updraft.

4) Fractional entrainment $\hat{\epsilon}$ and detrainment $\hat{\delta}$ rates

UNICON uses inertial buoyancy sorting to compute $\hat{\epsilon}$ and $\hat{\delta}$. During a vertical displacement of Δp, a certain amount of updraft air is mixed with the same amount of environmental air, producing a spectrum of mixtures between convective updraft ($\chi = 0$) and environmental air ($\chi = 1$) with a mass PDF of $P(\chi)$. In addition to the positively buoyant mixtures, UNICON entrains negatively buoyant mixtures with strong enough vertical velocities to rise over a critical distance $l_c = r_c \hat{z}_{\text{top}}(t - \Delta t)$, where r_c is a tunable constant and $\hat{z}_{\text{top}}(t - \Delta t)$ is the mean top height of the precedent updraft plumes. Appendix B details how to compute χ_c: the mixtures in $0 \le \chi \le \chi_c$ are entrained, while the other mixtures are detrained (Fig. 4). Following BMG04 and PB09, we can derive

$$\hat{\epsilon} = \hat{\epsilon}_o \left[2 \int_0^{\chi_c} \chi P(\chi)\, d\chi\right] \quad \text{and} \tag{33}$$

$$\hat{\delta} = \hat{\epsilon}_o \left[1 - 2 \int_0^{\chi_c} (1 - \chi) P(\chi)\, d\chi\right], \tag{34}$$

and by generalizing the previous studies, UNICON uses the symmetric beta distribution for $P(\chi)$,

$$P(\chi) = [\chi(1 - \chi)]^{p-1} \left[\frac{\Gamma(2p)}{\Gamma(p)\Gamma(p)}\right], \quad p > 0, \quad 0 \le \chi \le 1, \tag{35}$$

where $\Gamma(p) = (p - 1)!$ is a gamma function. If $p = 1$, $P(\chi) = 1$ and $\hat{\epsilon} = \hat{\epsilon}_o \chi_c^2$ and $\hat{\delta} = \hat{\epsilon}_o (1 - \chi_c)^2$, as used in BMG04 and PB09, while if $p = 2$, $P(\chi) = 6\chi(1 - \chi)$ and $\hat{\epsilon} = \hat{\epsilon}_o \chi_c^3 (4 - 3\chi_c)$ and $\hat{\delta} = \hat{\epsilon}_o (1 - 6\chi_c^2 + 8\chi_c^3 - 3\chi_c^4)$. Physically, for a given amount of air masses involved in the mixing, a larger p denotes a higher mixing efficiency between the updraft and environmental airs. Note that our $\hat{\epsilon}$ and $\hat{\delta}$ are complicated functions of $\hat{R}$, $\hat{B}$, $\hat{w}$, $\hat{q}_l$, $\hat{q}_i$, and $\widetilde{\text{RH}}_u$.

5) $\hat{S}_{q_t}$, $\hat{S}_{\theta_c}$, $\hat{S}_{\xi}$, $\hat{S}_{q_l}$, $\hat{S}_{q_i}$, $\hat{C}_u$, and $\hat{C}_v$

For simplicity, UNICON neglects the evaporation of convective precipitation within the updraft, so that the only source is the production of convective precipitation:

$$\hat{S}_{q_t} = \hat{S}_{q_l}^{\text{pr}} + \hat{S}_{q_i}^{\text{pr}}, \quad \text{and} \tag{36}$$

$$\hat{S}_{\theta_c} = -\left(\frac{1}{C_p \pi}\right)[L_v \hat{S}_{q_l}^{\text{pr}} + L_s \hat{S}_{q_i}^{\text{pr}}], \tag{37}$$

where $\hat{S}_{q_l}^{\text{pr}}$ and $\hat{S}_{q_i}^{\text{pr}}$ denote the conversion of cloud liquid droplets and ice crystals into convective precipitation, which are parameterized as

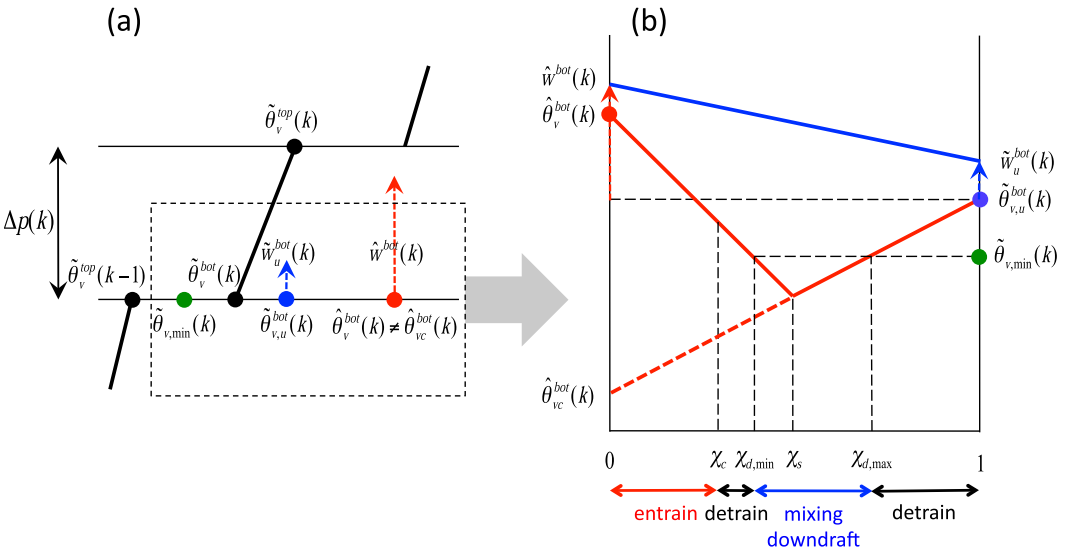

FIG. 4. Buoyancy sorting of a convective updraft. Because of the profile reconstruction (see appendix A), the profile of environmental scalar [thick black lines in (a)] is discontinuous at the model interfaces [e.g., $\tilde{\theta}_v^{\rm top}(k-1) \neq \tilde{\theta}_v^{\rm bot}(k)$]. At the base interface of the kth model layer, a convective updraft with virtual potential temperature $\hat{\theta}_v^{\rm bot}(k) \neq \hat{\theta}_{vc}^{\rm bot}(k)$ [where $\theta_{vc} \equiv (1 + 0.61q_t)\theta_c$ is condensate virtual potential temperature, q_t is total specific humidity, and θ_c is condensate potential temperature defined in section 2a] and vertical velocity $\hat{w}^{\rm bot}(k)$ (a red dot with an arrow) mixes with mixing environmental air [a blue dot with an arrow, $\tilde{\theta}_{v,u}^{\rm bot}(k) \neq \tilde{\theta}_v^{\rm bot}(k)$ and $\tilde{w}_u^{\rm bot}(k) \neq \tilde{w}^{\rm bot}(k)$], generating a spectrum of buoyancy [a red solid line in (b)] and vertical velocity [a blue solid line in (b)] as a function of the mass mixing fraction χ. Mixing environmental air can have nonzero vertical velocity [i.e., $\tilde{w}_u^{\rm bot}(k) = \Delta w_\Omega$ within the PBL]. Mixtures with positive buoyancy or sufficiently strong vertical velocity to rise over a critical distance l_c ($0 \le \chi \le \chi_c$) are entrained into the convective updraft. Strongly negatively buoyant mixtures with virtual potential temperature less than $\tilde{\theta}_{v,\min}(k) = (1-\lambda)\tilde{\theta}_v^{\rm top}(k-1) + \lambda\tilde{\theta}_v^{\rm bot}(k)$ ($\chi_{d,\min} \le \chi \le \chi_{d,\max}$) are converted into mixing downdrafts, and the remaining mixtures ($\chi_c \le \chi \le \chi_{d,\min}$ and $\chi_{d,\max} \le \chi \le 1$) are detrained into the current kth layer. See the text for details.

$$\hat{S}_{q_l}^{\rm pr} = -c_{\rm at}\max\left[\left(1 - \frac{\hat{q}_{c,\rm crit}}{\hat{q}_c}\right), 0\right]\hat{q}_l,$$

$$\hat{S}_{q_i}^{\rm pr} = -c_{\rm at}\max\left[\left(1 - \frac{\hat{q}_{c,\rm crit}}{\hat{q}_c}\right), 0\right]\hat{q}_i, \qquad (38)$$

where $c_{\rm at}$ is autoconversion efficiency, $\hat{q}_c \equiv \hat{q}_l + \hat{q}_i$ is the in-cumulus condensate, and $\hat{q}_{c,\rm crit}$ is the maximum in-cumulus condensate that a convective updraft can hold. The corresponding source of the tracer is computed as

$$\hat{S}_\xi = c_\xi(\hat{S}_{q_l}^{\rm pr} + \hat{S}_{q_i}^{\rm pr})\left(\frac{\hat{\xi}}{\hat{q}_c}\right), \qquad (39)$$

where c_ξ is a wet scavenging coefficient of tracers within the convective updraft. In principle, we need to compute the aerosol scavenging tendencies for cloudborne aerosols $\hat{\xi}_c$ (the activated and nucleated aerosols within cumulus liquid droplets and ice crystals) and interstitial aerosols $\hat{\xi}_i$ (the nonactivated aerosols outside of cumulus liquid droplets and ice crystals) and sum the two. However, without the aerosol activation and ice nucleation processes at the base of and within the cumulus (so-called secondary activation) and double-moment cumulus microphysics, current UNICON does not trace vertical evolution of individual $\hat{\xi}_c$ and $\hat{\xi}_i$. Thus, Eq. (39) is an approximation that should be refined in the future.

In contrast to q_t and θ_c, cloud condensates are not conserved scalars when phase changes occur. The sources of the cloud condensate within the convective updraft are

$$\hat{S}_{q_l} = \hat{S}_{q_l}^{\rm pr} + \left(\frac{\hat{q}_l^{\rm top} - \hat{q}_{l,\rm adi}^{\rm top}}{\Delta p}\right), \quad \hat{S}_{q_i} = \hat{S}_{q_i}^{\rm pr} + \left(\frac{\hat{q}_i^{\rm top} - \hat{q}_{i,\rm adi}^{\rm top}}{\Delta p}\right), \qquad (40)$$

where the second term on the rhs collectively represents the changes of $\hat{q}_l$ and $\hat{q}_i$ due to the adiabatic condensation, evaporation associated with the mixing with the mixing environmental air, and the freezing during upward motion. UNICON computes $\hat{q}_l^{\rm top}$ and $\hat{q}_i^{\rm top}$ from $\hat{\theta}_c^{\rm top}$ and $\hat{q}_t^{\rm top}$, while $\hat{q}_{l,\rm adi}^{\rm top}$ and $\hat{q}_{i,\rm adi}^{\rm top}$ are obtained by applying Eq. (26) to $\hat{\phi} = \hat{q}_l, \hat{q}_i$. Given the lack of two-moment cumulus

microphysics, UNICON computes $\hat{S}_{n_l}$ and $\hat{S}_{n_i}$ using the specified radii of cloud liquid droplets $\hat{r}_l$ and ice crystals $\hat{r}_i$ as $\hat{S}_{n_l} = \hat{S}_{q_l}[3/(4\pi\hat{r}_l^3\rho_l)]$ and $\hat{S}_{n_i} = \hat{S}_{q_i}[3/(4\pi\hat{r}_i^3\rho_i)]$ (and $\hat{n}_l$ and $\hat{n}_i$ are computed in the same way from $\hat{q}_l$ and $\hat{q}_i$ using the specified $\hat{r}_l$ and $\hat{r}_i$, respectively) where $\rho_l = 997\,\mathrm{kg\,m^{-3}}$ and $\rho_i = 500\,\mathrm{kg\,m^{-3}}$ are the densities of cloud liquid droplets and ice crystals, respectively. Note that the second process on the rhs does not change $\hat{\xi}$, although it induces conversion between $\hat{\xi}_c$ and $\hat{\xi}_i$.

The conversion term $\hat{C}_\phi$ is set to zero except for $\hat{C}_u$ and $\hat{C}_v$, which are parameterized following Wu and Yanai (1994) and Gregory et al. (1997) as

$$\hat{C}_u = c_m\tilde{\gamma}_u, \quad \hat{C}_v = c_m\tilde{\gamma}_v, \tag{41}$$

where $\tilde{\gamma}_u \equiv \Delta\tilde{u}/\Delta p$ and $\tilde{\gamma}_v \equiv \Delta\tilde{v}/\Delta p$ are the vertical gradients of the environmental horizontal wind in each layer, and the coefficient c_m measures the degree to which the horizontal momentum of the convective updraft adjusts to the environment during vertical motion without the mass exchange with the environment.

c. Convective downdraft

1) SOURCES

An individual convective updraft originating at the surface can generate three types of convective downdrafts (Fig. 3): a mixing downdraft generated from the mixing of the convective updraft with the mixing environmental air at the base interface of each layer; a top downdraft generated from the convective updraft at the top, where $\hat{B} < 0$ and $\hat{w} = 0$; and a constrained downdraft generated from the numerical requirement of $\hat{w} < \hat{w}_{\max}$ and $\sum_i \hat{a}^i < \hat{A}_{\max}$ at the top interface of each layer, where $\hat{w}_{\max}$ and $\hat{A}_{\max}$ are the maximum vertical velocity and the maximum net fractional area, respectively, that convective updraft can have. An individual convective updraft rising up to the kth layer from the surface can generate a maximum of $2k$ downdraft sources, consisting of k mixing downdrafts from the lowest to the cumulus top layers, one top downdraft in the cumulus top layer, and $k-1$ constrained downdrafts in all convective layers except the cumulus top layer. Each convective downdraft has its own downdraft mass flux ($\check{M}_m$, $\check{M}_t$, $\check{M}_c$) and a single value of scalar ($\check{\phi}_m$, $\check{\phi}_t$, $\check{\phi}_c$) at its origination level. The next subsection describes how these three downdraft sources are generated from the convective updraft.

(i) Mixing downdraft

According to the buoyancy sorting, only mixtures within the range $0 \le \chi \le \chi_c$ are entrained into a convective updraft. From the simple logical argument that negatively buoyant mixtures will sink, UNICON assumes that some of the nonentrained mixtures with $\theta_v(\chi) \le \tilde{\theta}_{v,\min}(k)$ (i.e., the mixtures within the range $\chi_c \le \chi_{d,\min} \le \chi \le \chi_{d,\max} \le 1$) are converted into a single mixing downdraft, while the remaining mixtures within the range $\chi_c \le \chi \le \chi_{d,\min}$ and $\chi_{d,\max} \le \chi \le 1$ are detrained into the layer k (Fig. 4 where k increases with height). Here, $\tilde{\theta}_{v,\min}(k)$ is the minimum of the environmental virtual potential temperature within and at the base interface of k,

$$\tilde{\theta}_{v,\min}(k) = \min[\tilde{\theta}_v^{\mathrm{top}}(k), \tilde{\theta}_v^{\mathrm{bot}}(k), (1-\lambda)\tilde{\theta}_v^{\mathrm{top}}(k-1) + \lambda\tilde{\theta}_v^{\mathrm{bot}}(k)], \tag{42}$$

where $0 \le \lambda \le 1$ and UNICON uses $\lambda = 0.5$. The mass flux and the mass flux–weighted mean conservative scalar of a single mixing downdraft are

$$\check{M}_m = 2\hat{f}_m\hat{M}^{\mathrm{bot}}\hat{\epsilon}_0\Delta p\int_{\chi_{d,\min}}^{\chi_{d,\max}} P(\chi)\,d\chi \quad \text{and} \tag{43}$$

$$\check{\phi}_m = \hat{\phi}^{\mathrm{bot}} + \left[\frac{\int_{\chi_{d,\min}}^{\chi_{d,\max}} \chi P(\chi)\,d\chi}{\int_{\chi_{d,\min}}^{\chi_{d,\max}} P(\chi)\,d\chi}\right](\tilde{\phi}_u^{\mathrm{bot}} - \hat{\phi}^{\mathrm{bot}}), \tag{44}$$

where $\hat{f}_m = \{\exp[(\hat{\epsilon}-\hat{\delta})\Delta p] - 1\}/[(\hat{\epsilon}-\hat{\delta})\Delta p]$ is a mass flux correction factor taking into account the vertical evolution of $\hat{M}$ during a vertical displacement of Δp, so that $\hat{f}_m\hat{M}^{\mathrm{bot}}$ is the mean $\hat{M}$ in Δp. Equation (44) is obtained from $\check{\phi}_m\int_{\chi_{d,\min}}^{\chi_{d,\max}} P(\chi)\,d\chi = \hat{\phi}^{\mathrm{bot}}\int_{\chi_{d,\min}}^{\chi_{d,\max}}(1-\chi)P(\chi)\,d\chi + \tilde{\phi}_u^{\mathrm{bot}}\int_{\chi_{d,\min}}^{\chi_{d,\max}}\chi P(\chi)\,d\chi$. UNICON computes $\chi_{d,\min}$ and $\chi_{d,\max}$ from the condition that $\theta_v(\chi) \le \tilde{\theta}_{v,\min}(k)$ (see Fig. 4b).

(ii) Top downdraft

The convective updraft at its top is negatively buoyant with zero vertical velocity, so that it sinks down from the top (i.e., it is converted into the downdraft) and is eventually detrained into the environment at its neutral buoyancy level. UNICON defines this downdraft as the top downdraft with $\check{M}_t$ and $\check{\phi}_t$ identical to the values of the convective updraft at its top (Fig. 3):

$$\check{M}_t = \hat{M}^{\mathrm{TOP}} \quad \text{and} \tag{45}$$

$$\check{\phi}_t = \hat{\phi}^{\mathrm{TOP}}, \tag{46}$$

where TOP denotes the updraft top where $\hat{w} = 0$. Thanks to the detailed dynamic treatment of the top downdraft and the mixing downdraft above the level of

neutral buoyancy (LNB), UNICON does not need a separate parameterization for penetrative entrainment at the cumulus top, such as the one used in PB09.

(iii) Constrained downdraft

UNICON imposes a constraint that $\hat{w}$ is smaller than the specified $\hat{w}_{\max}$. If $\hat{w} > \hat{w}_{\max}$, UNICON detrains the excessive updraft mass flux assuming $\hat{a}$ is not changed and resets $\hat{w} = \hat{w}_{\max}$. In addition, UNICON imposes a constraint that the net updraft fractional area is smaller than the specified maximum value $\hat{A}_{\max}$. If $\hat{A} = \sum_i \hat{a}^i \geq \hat{A}_{\max}$, the excessive updraft mass flux is proportionally detrained from the individual convective updraft. The sum of these numerically detrained updrafts at the top interface of individual layers forms the constrained downdraft with the mass flux $\check{M}_c$ and scalar $\check{\phi}_c$ computed as

$$\check{M}_c = \max\left[0, \left(1 - \frac{\hat{w}_{\max}}{\hat{w}^{\text{top}}}\right)\right]\hat{M}^{\text{top}} + \max\left[0, \left(1 - \frac{\hat{A}_{\max}}{\sum_i \hat{a}^{\text{top},i}}\right)\right]\hat{M}^{\text{top},-} \quad \text{and} \quad (47)$$

$$\check{\phi}_c = \hat{\phi}^{\text{top}}, \quad (48)$$

where $\hat{M}^{\text{top}}$ is the updraft mass flux before applying two constraints and $\hat{M}^{\text{top},-}$ is the updraft mass flux after applying the vertical velocity constraint (Fig. 3). Both constraints reduce $\hat{M}$, while the area constraint additionally decreases $\hat{R}$. UNICON uses the vertical velocity constraint to prevent the onset of unreasonably large $\hat{w}$ in association with the uncertainties in the parameterized a, b, and $\hat{\epsilon}$ in Eq. (28) and a coarse vertical resolution in typical GCMs.

2) VERTICAL EVOLUTION

Once generated, the vertical evolution of a convective downdraft ($\check{M}$, $\check{\phi}$, $\check{w}$) is controlled by the same equation set as the one used for a convective updraft [Eqs. (25), (26), and (28)] but with the following simplifying assumptions: $\check{\epsilon}$ and $\check{\delta}$ are externally specified, and a fixed buoyancy coefficient of $a = \frac{2}{3}$ is used [Eq. (29)]; a convective downdraft is mixed with the mean (not mixing) environmental air (i.e., $\tilde{\phi}_d = \tilde{\phi}$); a convective downdraft does not produce, but instead only evaporates, convective precipitation; and no constraints are imposed on $\check{w}$ and $\check{a}$. Within each layer, an individual downdraft is displaced down to the base interface, where it evaporates some of the convective precipitation. If $\check{\theta}_v^{\text{bot}}(k) < \tilde{\theta}_{v,\min}(k)$ after evaporation, a downdraft moves down into the next underlying layer and generates convective downdraft flux at that interface, but if $\check{\theta}_v^{\text{bot}}(k) \geq \tilde{\theta}_{v,\min}(k)$, it is detrained into the kth layer.

3) $\check{S}_{q_t}$, $\check{S}_{\theta_c}$, $\check{S}_{\xi}$, $\check{S}_{q_l}$, $\check{S}_{q_i}$, $\check{C}_u$, AND $\check{C}_v$

A convective downdraft evaporates some of the convective precipitation, and the associated sources of $\check{S}_{q_t}$ and $\check{S}_{\theta_c}$ are computed as

$$\check{S}_{q_t} = \check{S}_{q_v}^{e,R} + \check{S}_{q_v}^{e,S} \quad \text{and} \quad (49)$$

$$\check{S}_{\theta_c} = -\left(\frac{1}{C_p \pi}\right)\left(L_v \check{S}_{q_v}^{e,R} + L_s \check{S}_{q_v}^{e,S}\right), \quad (50)$$

where $\check{S}_{q_v}^{e,R}$ and $\check{S}_{q_v}^{e,S}$ are the evaporation and sublimation rates of convective rain and snow within the convective downdraft, computed as

$$\check{S}_{q_v}^{e,R} = \left(\frac{k_{e,R}}{\rho g \check{w}}\right)\left(1 - \frac{\check{q}_v}{\check{q}_s}\right)\sqrt{F_R/\check{a}} \quad \text{and}$$

$$\check{S}_{q_v}^{e,S} = \left(\frac{k_{e,S}}{\rho g \check{w}}\right)\left(1 - \frac{\check{q}_v}{\check{q}_s}\right)\sqrt{F_S/\check{a}}, \quad (51)$$

where $\check{w} \geq \check{w}_{\min}$ is the downdraft vertical velocity ($\check{w}_{\min}$ is a minimum downdraft vertical velocity); $\check{q}_s$ is the saturation specific humidity within the downdraft; F_R and F_S are the grid-mean convective rain and snow fluxes after snow melting, respectively; $\check{a}$ is the convective precipitation area [Eq. (85)]; and $k_{e,R}$ and $k_{e,S}$ are the evaporation and sublimation efficiencies of rain and snow. We impose the constraints that the amount of evaporated rain and sublimated snow within the downdraft during a vertical displacement of Δp ($\check{S}_{q_v}^{e,R}\Delta p$, $\check{S}_{q_v}^{e,S}\Delta p$) is smaller than $(\eta F_R)/(\check{M}N_d)$ and $(\eta F_S)/(\check{M}N_d)$, respectively, and the water vapor specific humidity within the downdraft after evaporation of precipitation cannot be larger than the wet-bulb specific humidity. Here, N_d is the number of mixing downdraft plumes and the factor η (conceptually, the ratio of the overlapping area between $\check{a}$ and $\hat{a}$ to $\check{a}$) specifies the maximum fraction of the convective precipitation that an individual downdraft can evaporate in each layer. Evaporation of precipitation within the top and constrained downdrafts are neglected. The corresponding source of the tracer is computed as

$$\check{S}_{\xi} = (\check{S}_{q_v}^{e,R} + \check{S}_{q_v}^{e,S})\left(\frac{F_{\xi}}{F_R + F_S}\right), \quad (52)$$

where F_{ξ} is the grid-mean tracer flux. The source for the convective cloud condensate within the downdraft is

$$\check{S}_{q_l} = \left(\frac{\check{q}_l^{\text{bot}} - \check{q}_{l,\text{adi}}^{\text{bot}}}{\Delta p}\right), \quad \check{S}_{q_i} = \left(\frac{\check{q}_i^{\text{bot}} - \check{q}_{i,\text{adi}}^{\text{bot}}}{\Delta p}\right), \tag{53}$$

which collectively represents the adiabatic evaporation, the evaporation associated with the mixing, and the melting of cloud ice during downward motion. UNICON computes $\check{q}_l^{\text{bot}}$ and $\check{q}_i^{\text{bot}}$ from $\check{\theta}_c^{\text{bot}}$ and $\check{q}_t^{\text{bot}}$, while $\check{q}_{l,\text{adi}}^{\text{bot}}$ and $\check{q}_{i,\text{adi}}^{\text{bot}}$ are obtained by applying Eq. (26) to $\check{\phi} = \check{q}_l$, $\check{q}_i$. Similar to a convective updraft, $\check{S}_{n_l}$ and $\check{S}_{n_i}$ are computed using the specified radii of cloud liquid droplets and ice crystals. Note that the above process does not change $\check{\xi}$. The conversion term $\check{C}_\phi$ is set to zero except for $\check{C}_u$ and $\check{C}_v$, which are parameterized as Eq. (41).

4) SINK: DETRAINMENT

According to the buoyancy sorting, the mixtures in $\chi_c \le \chi \le \chi_{d,\min}$ and $\chi_{d,\max} \le \chi \le 1$ are detrained into the environment (Fig. 4). The mass flux and the mass flux–weighted mean conservative scalar of the detrained mixtures from the buoyancy sorting of an individual convective updraft are

$$\hat{M}_r = 2\hat{f}_m \hat{M}^{\text{bot}} \hat{\epsilon}_o \Delta p \left[\int_{\chi_c}^{\chi_{d,\min}} P(\chi)\, d\chi + \int_{\chi_{d,\max}}^{1} P(\chi)\, d\chi\right]$$

and

$$\hat{\phi}_r = \hat{\phi}^{\text{bot}} + \left[\frac{\displaystyle\int_{\chi_c}^{\chi_{d,\min}} \chi P(\chi)\, d\chi + \int_{\chi_{d,\max}}^{1} \chi P(\chi)\, d\chi}{\displaystyle\int_{\chi_c}^{\chi_{d,\min}} P(\chi)\, d\chi + \int_{\chi_{d,\max}}^{1} P(\chi)\, d\chi}\right] \times (\tilde{\phi}_u^{\text{bot}} - \hat{\phi}^{\text{bot}}). \tag{55}$$

A convective downdraft can also be detrained into the environment. During vertical displacement, a downdraft is mixed with mean environmental air at the rates of $\check{\epsilon}$ and $\check{\delta}$. The net amount of downdraft mass flux and the mass flux–weighted conservative scalar detrained from the downdraft is

$$\check{M}_r = \check{f}_m \check{M}^{\text{top}} \check{\delta} \Delta p + \mu \check{M}^{\text{bot}} \quad \text{and} \tag{56}$$

$$\check{\phi}_r = [(1/2)(\check{\phi}^{\text{top}} + \check{\phi}^{\text{bot}}) \check{f}_m \check{M}^{\text{top}} \check{\delta} \Delta p + \check{\phi}^{\text{bot}} \mu \check{M}^{\text{bot}}] / \check{M}_r, \tag{57}$$

with $\check{f}_m = \{\exp[(\check{\epsilon} - \check{\delta})\Delta p] - 1\}/[(\check{\epsilon} - \check{\delta})\Delta p]$ and

$$\mu = \begin{cases} 1, & \text{if} \quad \check{\theta}_v^{\text{bot}} > \tilde{\theta}_{v,\min} \quad \text{or} \quad \check{M}^{\text{bot}} < \check{M}_{\min}, \\ 0, & \text{if} \quad \check{\theta}_v^{\text{bot}} \le \tilde{\theta}_{v,\min} \quad \text{and} \quad \check{M}^{\text{bot}} \ge \check{M}_{\min}, \end{cases} \tag{58}$$

where we set $\check{M}_{\min} = 1 \times 10^{-5}\,\text{kg}\,\text{m}^{-2}\,\text{s}^{-1}$. Finally, the net amount of the mass and the mean conservative scalar of the detrained air (M_r, ϕ_r) that is used as a part of the mixing environmental air for the mixing with the convective updraft at the next time step [Eq. (78)] is

$$M_r = \sum_i \hat{M}_r^i + \sum_j \check{M}_r^j \quad \text{and} \tag{59}$$

$$\phi_r = \left(\sum_i \hat{\phi}_r^i \hat{M}_r^i + \sum_j \check{\phi}_r^j \check{M}_r^j\right) \Big/ M_r, \tag{60}$$

where i and j are the indices denoting individual convective updrafts and downdrafts, respectively.

d. *Parameterization of cold pools*

If forced by sufficient evaporative cooling of precipitation, a convective downdraft can penetrate down into the PBL across the inversion barrier at the PBL top. The virga frequently observed over the continents during the midafternoon in summer is a visualization of this negatively buoyant convective downdraft, which generates a cold pool within the PBL. We assume that the properties of a convective updraft at the surface and the mixing environmental air within and above the PBL are modulated by the subgrid mesoscale organized flow driven by the cold pool. UNICON parameterizes the cold pool by dividing the horizontal grid within the PBL into the portion into which evaporation-driven convective downdrafts are subsiding (a_D) and the remaining portion from which convective updrafts are rising ($a_U = 1 - a_D$) and applying separate budget equations to each of the a_U and a_D regions. The resulting budget equations for the mass and conservative scalars averaged over the PBL depth in the a_U and a_D regions are (see appendix C for details)

$$\begin{aligned} \frac{\partial a_U}{\partial t} = &- U_{\text{PBL}} \frac{\partial a_U}{\partial x} - V_{\text{PBL}} \frac{\partial a_U}{\partial y} + (\delta_c - \epsilon_c) \\ &- \frac{g}{\Delta p_h}\left(\sum_i \hat{M}_h^i - \sum_j \check{M}_{U,h}^j\right) \\ &- \frac{g}{\Delta p_h}\left[\sum_j (\check{M}_{D,h}^j + \check{M}_{U,h}^j) - \sum_i \hat{M}_h^i\right] a_U, \end{aligned} \tag{61}$$

$$\frac{\partial a_D}{\partial t} = -U_{\rm PBL}\frac{\partial a_D}{\partial x} - V_{\rm PBL}\frac{\partial a_D}{\partial y} + (\epsilon_c - \delta_c) + \frac{g}{\Delta p_h}\sum_j \check{M}^j_{D,h} - \frac{g}{\Delta p_h}\left[\sum_j (\check{M}^j_{D,h} + \check{M}^j_{U,h}) - \sum_i \hat{M}^i_h\right] a_D, \tag{62}$$

$$\begin{aligned}\frac{\partial}{\partial t}(\Delta\phi_U) = {} & -U_{\rm PBL}\frac{\partial}{\partial x}(\Delta\phi_U) - V_{\rm PBL}\frac{\partial}{\partial y}(\Delta\phi_U)\\ & - \frac{g}{\Delta p_h}\left\{\sum_j\left[\check{M}^j_{D,h}(\check{\phi}^j_{D,h} - \phi_{\rm PBL}) - \frac{a_D}{a_U}\check{M}^j_{U,h}(\check{\phi}^j_{U,h} - \phi_{\rm PBL})\right] + \frac{a_D}{a_U}\sum_i \hat{M}^i_h(\hat{\phi}^i_h - \phi_{\rm PBL})\right\}\\ & + g\left\langle \frac{a_D}{a_U}\sum_i \hat{M}^i\hat{S}^i_\phi + \sum_j\left(\frac{a_D}{a_U}\check{M}^j_U\check{S}^j_{\phi,U} - \check{M}^j_D\check{S}^j_{\phi,D}\right)\right\rangle_0^h + \langle (S_{e,U} - \overline{S}_e)_\phi\rangle_0^h\\ & - \left\{\frac{\delta_c}{a_D a_U} + \frac{g}{\Delta p_h}\left[\sum_j\left(\check{M}^j_{G,h} + \frac{1}{a_U}\check{M}^j_{U,h}\right) + \rho_s C_d V_s + \rho_h W_{e,h} - \frac{1}{a_U}\sum_i \hat{M}^i_h\right]\right\}\Delta\phi_U, \quad \text{and}\end{aligned} \tag{63}$$

$$\begin{aligned}\frac{\partial}{\partial t}(\Delta\phi_D) = {} & -U_{\rm PBL}\frac{\partial}{\partial x}(\Delta\phi_D) - V_{\rm PBL}\frac{\partial}{\partial y}(\Delta\phi_D)\\ & + \frac{g}{\Delta p_h}\left\{\sum_j\left[\frac{a_U}{a_D}\check{M}^j_{D,h}(\check{\phi}^j_{D,h} - \phi_{\rm PBL}) - \check{M}^j_{U,h}(\check{\phi}^j_{U,h} - \phi_{\rm PBL})\right] + \sum_i \hat{M}^i_h(\hat{\phi}^i_h - \phi_{\rm PBL})\right\}\\ & + g\left\langle \sum_j\left(\frac{a_U}{a_D}\check{M}^j_D\check{S}^j_{\phi,D} - \check{M}^j_U\check{S}^j_{\phi,U}\right) - \sum_i \hat{M}^i\hat{S}^i_\phi\right\rangle_0^h + \langle (S_{e,D} - \overline{S}_e)_\phi\rangle_0^h\\ & - \left\{\frac{\epsilon_c}{a_D a_U} + \frac{g}{\Delta p_h}\left[\sum_j\left(\frac{1}{a_D}\check{M}^j_{D,h} + \check{M}^j_{G,h}\right) + \rho_s C_d V_s + \rho_h W_{e,h}\right]\right\}\Delta\phi_D,\end{aligned} \tag{64}$$

where $\phi = q_t, \theta_c, u, v, \xi$; the superscripts i and j are the indices denoting individual convective updrafts and downdrafts, respectively; the subscript h denotes the value at the PBL top; the angle brackets $\langle\cdot\rangle_0^h$ are the vertical average over the PBL depth with 0 and h denoting the surface and the PBL-top height, respectively; $\phi_{\rm PBL} \equiv \langle\tilde{\phi}\rangle_0^h$ is the environmental scalar averaged over the PBL; $U_{\rm PBL} \equiv \langle\tilde{u}\rangle_0^h$ and $V_{\rm PBL} \equiv \langle\tilde{v}\rangle_0^h$ are the environmental zonal and meridional winds averaged over the PBL; ϵ_c and δ_c denote the lateral entrainment and detrainment rates between a_D and a_U (here, subscript c stands for the cold pool), respectively; $\Delta p_h > 0$ is the depth of the PBL; $(\check{M}_U, \check{M}_D, \check{M}_G)$ and $(\check{\phi}_U, \check{\phi}_D, \check{\phi}_G)$ denote the mass fluxes and the scalars of the convective downdrafts that sink exclusively into a_U and a_D and over the entire grid, respectively; $(S_{e,U}, S_{e,D}, \overline{S}_e)$ are the sources within the environment averaged over a_U and a_D and the entire grid, respectively; C_d is a dimensionless surface exchange coefficient; V_s is the horizontal wind speed in the lowest model layer; $W_{e,h}$ is the entrainment rate at the PBL top computed from the separate PBL scheme; and $\Delta\phi_U \equiv \phi_U - \phi_{\rm PBL}$ ($\Delta\phi_D \equiv \phi_D - \phi_{\rm PBL}$) is the difference in conservative scalar between the a_U (a_D) region and the grid mean within the PBL (see Fig. 5). In the above equations, all the mass fluxes are relative mass fluxes with $\check{M} > 0$. As detailed in appendix C, $\check{M}_{D,h}$ is defined as the mixing downdraft that has originated from above the PBL top, is accompanied by nonzero precipitation flux at the PBL-top interface, and can sink all the way down to the lowest model interface above the surface. We parameterize $\epsilon_c = \epsilon_* a_D$ and $\delta_c = \delta_* a_D$ by assuming a stronger mixing between the cold pool and the ambient air as the cold pool becomes larger. The difference between the environmental sources averaged over a_U (a_D) and over the grid are

$$(S_{e,U} - \overline{S}_e)_{q_t} = \frac{1}{a_U}\sum_i [(\ddot{a}^i_U - \ddot{a}^i a_U)(\ddot{E}^i_R + \ddot{E}^i_S)], \tag{65}$$

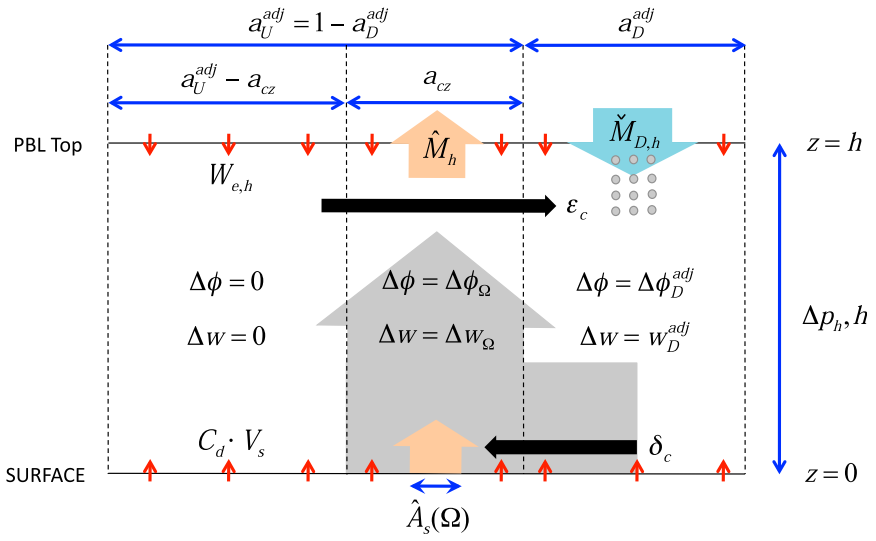

FIG. 5. Parameterization of subgrid cold pool and mesoscale organized flow within the PBL. The grid column within the PBL is divided into three bulk portions: $a_D^{\rm adj}$ into which convective downdrafts accompanied by convective precipitation penetrate (i.e., a cold pool), $a_{\rm cz} = c_\Omega \hat{A}_s(\Omega)$ is the upflow branch of subgrid mesoscale organized flow, and the remaining $a_U^{\rm adj} - a_{\rm cz}$ where no mesoscale perturbation exists with respect to the grid mean (i.e., $\Delta\phi \equiv \phi - \phi_{\rm PBL} = 0$, $\Delta w = 0$). The cold pool $a_D^{\rm adj}$ is forced by evaporation of convective precipitation and convective downdrafts $\check{M}_{D,h}$ that exclusively sink down into $a_D^{\rm adj}$, while damped by the surface flux and the entrainment flux at the PBL top ($C_d V_s$ is the transfer velocity at the surface and $W_{e,h}$ is the entrainment rate at the PBL top). Lateral mass exchange between the cold pool and the ambient mean environmental air (ϵ_c, δ_c) is allowed. All the parameterized convective updrafts with a net fractional area at the surface $\hat{A}_s(\Omega)$ are assumed to rise through $a_{\rm cz}$ within the PBL, so that the properties of the source updraft at the surface and mixing environmental air within the PBL are perturbed by $\Delta\phi_\Omega$ [Eqs. (73) and (78)] and Δw_Ω [Eqs. (74), (78), and (B2)]. In addition, UNICON imposes mesoscale perturbations on the fractional area [Eq. (75)] and the radius [Eqs. (76) and (77)] of convective updraft plumes at the surface. See sections 2d and 2e for details.

$$(S_{e,U} - \overline{S}_e)_{\theta_c} = -\left(\frac{1}{C_p \pi}\right)\frac{1}{a_U}\sum_i [(\ddot{a}_U^i - \ddot{a}^i a_U)(L_v \ddot{E}_R^i + L_s \ddot{E}_S^i)] + \frac{1}{a_U}\sum_i \left[(\check{a}_U^i - \check{a}^i a_U)\left(\tilde{a}\frac{\partial \tilde{\theta}_c}{\partial t}\right)_{\rm mlt}^i \left(\frac{1}{\check{a}^i}\right)\right], \quad \text{and} \tag{66}$$

$$(S_{e,D} - \overline{S}_e)_\phi = -\left(\frac{a_U}{a_D}\right)(S_{e,U} - \overline{S}_e)_\phi, \tag{67}$$

where the subscripts q_t and θ_c are total specific humidity and condensate potential temperature, respectively, with ϕ denoting any conservative scalars; $(\tilde{a}\partial\tilde{\theta}_c/\partial t)_{\rm mlt}$ is the grid-mean tendency of θ_c due to snow melting [Eq. (87)]; $\ddot{E}_R$ and $\ddot{E}_S$ are the localized rain evaporation and snow sublimation tendencies within the evaporation area, respectively [Eq. (81)]; $\ddot{a}_U$ is the overlapping area between the evaporation area $\ddot{a}$ [Eq. (80)] and a_U; and $\check{a}_U$ is the overlapping area between the precipitation area $\check{a}$ [Eq. (85)] and a_U:

$$\ddot{a}_U^i = (1-\beta)\ddot{a}^i a_U + \beta \max(\ddot{a}^i + a_U - 1, 0) \quad \text{and} \tag{68}$$

$$\check{a}_U^i = (1-\beta)\check{a}^i a_U + \beta \max(\check{a}^i + a_U - 1, 0), \tag{69}$$

where β is an overlapping parameter between $\ddot{a}$ (or $\check{a}$) and a_U with $\beta = 0$ (1) for random (minimum) overlap. We can also interpret β as an overlapping parameter between $\ddot{a}$ (or $\check{a}$) and a_D with $\beta = 0$ (1) for random (maximum) overlap. In case of the random overlap, Eqs. (65)–(67) become zero, as expected. The corresponding sources for the tracers are computed in a way similar to Eq. (52) by noting that snow melting does not alter ξ.

Each of Eqs. (61)–(64) is a first-order linear differential equation with a forcing term f and a linear damping (or amplifying) term, $\partial y/\partial t = f - y/\tau$, where τ is a damping (or amplifying) time scale and $y = a_U, a_D, \Delta\phi_U, \Delta\phi_D$. In the numerical code, we prognose a_D and $\Delta\phi_U$, from which a_U and $\Delta\phi_D$ are computed by using $a_U = 1 - a_D$ and $a_U\Delta\phi_U + a_D\Delta\phi_D = 0$. In order to obtain a stable solution with a long Δt in GCM, Eqs. (61)–(64) are solved analytically by treating $\delta_* - \epsilon_*$ as a part of τ^{-1} in Eq. (62).

However, the advection term is numerically treated by the separate grid-scale advection scheme. We force $0 \le a_D \le 1 - \hat{A}_{\max}$ by adding a corrective detrainment to the original δ_c whenever the prognosed a_D becomes larger than $1 - \hat{A}_{\max}$.

Although a single $\Delta\phi_D$ is computed, it is reasonable to assume that $\Delta\phi_D$ has internal variability since the cold pool is driven by the various convective downdrafts generated from various convective updrafts. The area PDF of the cold pool, $P_c(x)$, is assumed to follow a Gaussian distribution, where $x \equiv -\delta\theta_{v,D} = \theta_{v,\mathrm{PBL}} - \theta_{v,D}$. A convective downdraft always induces positive buoyancy flux at the PBL top. Snow melting and the evaporation of precipitation within the convective downdraft and the environment additionally force $\Delta\theta_{v,D} \le 0$, where $\Delta\theta_{v,D}$ is computed from $\Delta\phi_D$. Thus, the assumption of a half-Gaussian distribution $P_c(x)$ in the range of $x \ge 0$ is a valid approximation. From two normalization conditions of $a_D = \int_0^\infty P_c(x)\,dx$ and $\Delta\theta_{v,D} = -[\int_0^\infty P_c(x)x\,dx]/a_D$, we can obtain $P_c(x) = [(2a_D)/(\sigma\sqrt{2\pi})]\exp[-(1/2)(x/\sigma)^2]$ where $\sigma = -\sqrt{\pi/2}\Delta\theta_{v,D}$ is the width of the distribution. The final cold pool area a_D^{adj} is defined as the area occupied by the elements with $x \ge x^{\mathrm{cri}} \equiv -\delta\theta_{v,D}^{\mathrm{cri}}$,

$$a_D^{\mathrm{adj}} = a_D\left[1 - \mathrm{erf}\left(\frac{\nu}{\sqrt{\pi}}\right)\right], \tag{70}$$

and then $\Delta\theta_{v,U}^{\mathrm{adj}} \equiv \theta_{v,U}^{\mathrm{adj}} - \theta_{v,\mathrm{PBL}}$ and $\Delta\theta_{v,D}^{\mathrm{adj}} \equiv \theta_{v,D}^{\mathrm{adj}} - \theta_{v,\mathrm{PBL}}$ are computed as

$$\Delta\theta_{v,U}^{\mathrm{adj}} = \Delta\theta_{v,U}\left(\frac{a_U}{a_U^{\mathrm{adj}}}\right)\exp\left(-\frac{\nu^2}{\pi}\right),$$

$$\Delta\theta_{v,D}^{\mathrm{adj}} = \Delta\theta_{v,D}\left(\frac{a_D}{a_D^{\mathrm{adj}}}\right)\exp\left(-\frac{\nu^2}{\pi}\right), \tag{71}$$

where $\nu \equiv \delta\theta_{v,D}^{\mathrm{cri}}/\Delta\theta_{v,D}$, and the same adjustment is applied for the other conservative scalars—$\phi = q_t, \theta_c, u, v, \xi$—using the same ν.

e. Subgrid mesoscale convective organization

We define the following nondimensional quantity, mesoscale convective organization:

$$\Omega \equiv \left(\frac{a_D^{\mathrm{adj}}}{1 - \hat{A}_{\max}}\right), \quad 0 \le \Omega \le 1, \tag{72}$$

and since $0 \le a_D^{\mathrm{adj}} \le 1 - \hat{A}_{\max}$ owing to the corrective detrainment (see section 2d) and Eq. (70), it is always guaranteed that $0 \le \Omega \le 1$. In nature, the outflow detrained from the cold pool spreads out near the surface, collides with other outflows driven by other cold pools, and is eventually converted into the upflow (see Fig. 5). UNICON assumes that any perturbations of thermodynamic scalars driven by the cold pool are confined in the cold pool and in the colliding zones of the outflows a_{cz}, instead of over the entire region of a_U^{adj}, and a_{cz} is a linear function of the net updraft fractional area at the surface, $a_{cz} = c_\Omega \hat{A}_s(\Omega)$. Using the Boussinesq approximation, the available potential energy (APE) corresponding to the horizontal density perturbation, $\theta_v' \equiv \theta_{v,U}^{\mathrm{adj}} - \theta_{v,D}^{\mathrm{adj}} \ge 0$, associated with the cold pool within the PBL [where $\theta_{v,U}^{\mathrm{adj}}$ and $\theta_{v,D}^{\mathrm{adj}}$ are computed in Eq. (71)] is $\mathrm{APE} = (1/2)(g/\theta_{v,\mathrm{ref}})ha_D^{\mathrm{adj}}a_U^{\mathrm{adj}}\theta_v'$, where $\theta_{v,\mathrm{ref}} = 300\,\mathrm{K}$ is the reference virtual potential temperature and h is the depth of the PBL. In the case that the upflow perturbations are confined in a_{cz} not over a_U^{adj}, as is being assumed, it becomes $\mathrm{APE}_{cz} = (1/2)(g/\theta_{v,\mathrm{ref}})ha_D^{\mathrm{adj}}a_{cz}\theta_{v,cz}'$, where $\theta_{v,cz}' \equiv \theta_{v,cz} - \theta_{v,D}^{\mathrm{adj}} = \theta_v'(a_U^{\mathrm{adj}}/a_{cz})(a_D^{\mathrm{adj}} + a_{cz})$. UNICON assumes that a certain fraction k_* of the APE_{cz} is converted into the mesoscale kinetic energy through a convective overturning process over the areas of a_{cz} and a_D^{adj}. From the conservation principles of the mesoscale vertical momentum, $w_{cz}a_{cz} + w_D^{\mathrm{adj}}a_D^{\mathrm{adj}} = 0$, and the mesoscale kinetic energy, $w_{cz}^2a_{cz} + (w_D^{\mathrm{adj}})^2a_D^{\mathrm{adj}} = 2k_*\mathrm{APE}_{cz}$, where $w_{cz} \ge 0$ and $w_D^{\mathrm{adj}} \le 0$ are the mesoscale vertical velocities in the a_{cz} and a_D^{adj}, respectively, and by assuming that $\hat{A}_s(\Omega)$ decreases linearly with Ω with $\hat{A}_s|_{\Omega=1} = \hat{A}_{\max}\hat{A}_s|_{\Omega=0}$ [Eq. (75)], we can derive the cold pool–driven perturbations for conservative scalars $\Delta\phi_\Omega$ [Eq. (18)] and the vertical velocity [$\Delta w_\Omega = w_{cz}$; Eq. (18)] of the convective updraft at the surface confined in a_{cz} as follows:

$$\Delta\phi_\Omega = \left(\frac{\Delta\phi_U^{\mathrm{adj}}}{c_\Omega\hat{A}_s|_{\Omega=0}}\right) \quad \text{and} \tag{73}$$

$$\Delta w_\Omega = a_D^{\mathrm{adj}}\left[\left(\frac{g}{\theta_{v,\mathrm{ref}}}\right)\left(\frac{k_*h\theta_v'}{c_\Omega\hat{A}_s|_{\Omega=0}}\right)\right]^{1/2}, \tag{74}$$

where $1 \le c_\Omega \le \hat{A}_s^{-1}|_{\Omega=0}$; that is, $\hat{A}_s(\Omega) \le a_{cz} \le a_U^{\mathrm{adj}}(\Omega)$, since all convective updrafts parameterized by UNICON are equally modulated by $\Delta\phi_\Omega$ and Δw_Ω [Eq. (18)] at the surface [i.e., $a_{cz} \ge \hat{A}_s(\Omega)$], and UNICON simulates subgrid mesoscale flow within each grid column [i.e., $a_{cz} \le a_U^{\mathrm{adj}}(\Omega)$]. If $\Omega \to 0$, both $\Delta\phi_\Omega$ and Δw_Ω approach to zero, as expected, since $\Delta\phi_U^{\mathrm{adj}} \to 0$ and $a_D^{\mathrm{adj}} \to 0$.

UNICON assumes that Ω also controls the macrophysics of the convective updraft and the mixing environmental air as well as the thermodynamic properties of the convective updraft at the surface. UNICON has three important unknown variables that should be appropriately specified or parameterized: 1) $\hat{A}_s$ [the net updraft fractional area at the surface; Eq. (19)], 2) R_o [the intercept radius of the updraft plume at the surface; Eq. (23)] and σ_R [the standard deviation of the updraft plume radius at the surface; Eq. (23)], and 3) $\tilde{\phi}_u$ [the

mixing environmental air of the convective updraft; Eq. (26)]. In UNICON, $\hat{A}_s$ affects the magnitude of the updraft mass flux, R_o and σ_R control the amount of the mixing [Eqs. (23) and (31)], and $\tilde{\phi}_u$ influences the degree of dilution of the convective updraft plume, all of which are important components in the parameterization of convection. UNICON assumes that these four variables are the functions of Ω:

$$\hat{A}_s(\Omega) = \hat{A}_s|_{\Omega=0} + \Omega \times (\hat{A}_s|_{\Omega=1} - \hat{A}_s|_{\Omega=0}) = \hat{A}_s|_{\Omega=0} \times [1 - \Omega \times (1 - \hat{A}_{\max})], \quad (75)$$

$$R_o(\Omega) = R_o|_{\Omega=0} + \Omega^{\gamma} \times (R_o|_{\Omega=1} - R_o|_{\Omega=0}), \quad (76)$$

$$\sigma_R(\Omega) = \sigma_R|_{\Omega=0} + \Omega^{\gamma} \times (\sigma_R|_{\Omega=1} - \sigma_R|_{\Omega=0}), \quad \text{and} \quad (77)$$

$$\tilde{\phi}_u(z,t) = \begin{cases} \tilde{\phi}(z,t) + \Delta\phi_{\Omega}, & \text{if} \quad z < h, \\ \tilde{\phi}(z,t) + \Omega_{\epsilon} \times [\phi_r(z,t-\Delta t) - \tilde{\phi}(z,t-\Delta t)], & \text{if} \quad z > h, \end{cases} \quad (78)$$

where $R_o|_{\Omega=0} \le R_o|_{\Omega=1}$, $\sigma_R|_{\Omega=0} \le \sigma_R|_{\Omega=1}$, $\gamma > 0$, $\Delta\phi_{\Omega}$ is from Eq. (73), $\tilde{\phi}(z, t)$ and $\tilde{\phi}(z, t-\Delta t)$ are the mean environmental scalar at the current and previous time steps, respectively, and $\phi_r(z, t-\Delta t)$ is the mean scalar of the detrained air at the previous time step [Eq. (60)]. The second equality of Eq. (75) is obtained by assuming $\hat{A}_s|_{\Omega=1} = \hat{A}_{\max} \times \hat{A}_s|_{\Omega=0}$ as mentioned before. Note that Δw_{Ω} defined in Eq. (74) for the initialization of the convective updrafts at the surface is also used in Eq. (78) within the PBL ($\phi = w$) in order to compute $\hat{w}(z)$ [Eq. (27)] and the updraft buoyancy sorting (see appendix B). In Eq. (78), $\Omega_{\epsilon} \equiv \min(\Omega, \Omega^*)$ with $\Omega^* \equiv M_r(z, t-\Delta t)/\sum_i(\hat{f}^i_m \hat{M}^{\text{bot},i} \hat{\epsilon}^i_o \Delta p)$ where $M_r(z, t-\Delta t)$ is the mass flux of detrained air at the previous time step [Eq. (59)] and the denominator is total amount of updraft air involved in the mixing at the current time step. We use the constraint of $\Omega_{\epsilon} = \min(\Omega, \Omega^*)$ because our mixing assumption requires that during a vertical displacement of Δp, a certain amount of updraft air [$\Delta\hat{M}_{\text{mix}} = \sum_i(\hat{f}^i_m \hat{M}^{\text{bot},i} \hat{\epsilon}^i_o \Delta p)$] is mixed with the same amount of mixing environmental air, so that the degree to which the convective updraft is mixed with the detrained air should be bound by the amount of the available detrained air [$M_r(z, t-\Delta t)$]. In the limit of $\Delta t \to 0$, the second line of Eq. (78) becomes $\tilde{\phi}_u(z, t) = (1-\Omega_{\epsilon})\tilde{\phi}(z, t) + \Omega_{\epsilon}\phi_r(z, t)$, which provides an alternative definition of Ω_{ϵ}: the probability for the convective updraft to preferentially rise into the horizontal spots occupied by the detrained air. In this sense, $\Omega_{\epsilon} = 0$ denotes the random rising since $\phi_r(z, t)$ is a part of $\tilde{\phi}(z, t)$. Equations (75)–(78) indicate that as convection becomes more organized, the updraft fractional area decreases, the mean and the variance of the updraft-plume radius increase, and an individual updraft plume rises through the mesoscale upflows generated by the colliding outflows of the cold pools within the PBL, and into the preceeding updraft plume's trajectory above the PBL, in line with the approach suggested by Mapes and Neale (2011).

f. Sources within the environment

In order to compute the grid-mean tendencies of all scalars $\phi = q_t, \theta_c, u, v, \xi, q_v, q_l, q_i, n_l, n_i$, UNICON uses Eq. (17), which guarantees the conservation of the column-integrated grid-mean conservative scalar I_{ϕ}—a mandatory requirement for GCM parameterization—if the column-integrated sources [$\hat{S}_{\phi}$, $\check{S}_{\phi}$, $(\partial\tilde{\phi}/\partial t)_s$] are correctly incorporated into the computation of the vertical evolution of the convective updraft and downdraft plumes and the precipitation and tracer fluxes at the surface. The last term in Eq. (17) is the source within the environment. If $\phi = q_t, \theta_c, q_v, \xi$, this environmental source consists of evaporation of convective rain and snow [evp in Eq. (79) for $\phi = q_t, \theta_c, q_v, \xi$], snow melting (mlt for $\phi = \theta_c$), and dissipation heating of the mean kinetic energy (dis for $\phi = \theta_c$):

$$\left(\tilde{a}\frac{\partial\tilde{\phi}}{\partial t}\right)_s = \left(\tilde{a}\frac{\partial\tilde{\phi}}{\partial t}\right)_{\text{evp}} + \left(\tilde{a}\frac{\partial\tilde{\phi}}{\partial t}\right)_{\text{mlt}} + \left(\tilde{a}\frac{\partial\tilde{\phi}}{\partial t}\right)_{\text{dis}}, \quad (79)$$

and each of these terms will be discussed in detail in the following sections. Environmental source for the other scalars is zero.

In UNICON, all convective microphysical processes—production of convective precipitation within the updraft at the top interface, evaporation of convective precipitation within the environment, snow melting within the environment at the base interface, and evaporation of convective precipitation within the downdraft at the base interface—are treated in an isolated way for each convective updrafts, so that the precipitation flux generated from the ith updraft segment does not fall into the other updrafts and the downdrafts generated from the non-ith updraft segment. This approach is analogous to assuming that cumulus and stratus do not see each other in the precipitation production: convective precipitation flux

falling into the stratus does not generate the stratiform precipitation by accretion and vice versa. This independent precipitation approximation is justifiable since UNICON assumes that the sum of all the updraft fractional areas, $\hat{A} = \sum_i \hat{a}^i$ is smaller than $\hat{A}_{\max} \ll 1$.

1) Evaporation of convective precipitation

An individual convective updraft generates a profile of grid-mean production rates of convective rain ($P_R = g\hat{M}\hat{S}^{\rm pr}_{q_l}$) and snow ($P_S = g\hat{M}\hat{S}^{\rm pr}_{q_i}$) and corresponding grid-mean rain (F_R) and snow fluxes (F_S) from the updraft top to the surface. The convective rain and snow fluxes within the precipitation area $\breve{a}^{\rm top}$ at the top interface of an individual layer can fall into any region of convective updraft $\hat{a}$, convective downdraft $\breve{a}$ (which is assumed to be zero as discussed in section 2a), stratus a_s, and clear areas ($a_r = 1 - \sum_i \hat{a}^i - \sum_j \breve{a}^j - a_s$) at the layer midpoint. Using the diagnosed velocity profiles of a convective updraft [$\hat{u}(z)$, $\hat{v}(z)$, $\hat{w}(z)$], UNICON computes the horizontal shift of the center of the updraft plume from the surface: $\hat{x}(z) = \int_0^z \{[\hat{u}(z) - \hat{u}(0)]/\hat{w}(z)\}\, dz$ and $\hat{y}(z) = \int_0^z \{[\hat{v}(z) - \hat{v}(0)]/\hat{w}(z)\}\, dz$ from $\hat{x}(0) = 0$ and $\hat{y}(0) = 0$. The overlapping area $\hat{a}^p_{\rm sat}$ between $\breve{a}^{\rm top}$ and $\hat{a}_{\rm sat}$ (a saturated $\hat{a}$; i.e., $\hat{a}_{\rm sat} = \hat{a}$ if the updraft is saturated while $\hat{a}_{\rm sat} = 0$ if the updraft is unsaturated) is computed by geometry using $(\hat{x}, \hat{y})$, $(\breve{x}^{\rm top}, \breve{y}^{\rm top})$ [the center coordinate of $\breve{a}^{\rm top}$ computed in Eq. (86)] and $P_n(\alpha)$ [Eq. (24)] assuming that both $\breve{a}^{\rm top}$ and $\hat{a}_{\rm sat}$ have the shape of a disk in each layer [i.e., $\breve{a}^{\rm top} = \pi\breve{R}^2 P_n(\alpha)\Delta\alpha$ and $\hat{a}_{\rm sat} = \pi\hat{R}^2_{\rm sat} P_n(\alpha)\Delta\alpha$, where $\breve{R}$ and $\hat{R}_{\rm sat}$ are the radii of the convective precipitation and the saturated convective updraft, respectively]. The evaporation area of convective precipitation $\ddot{a}$ is computed as the overlapping area between $\breve{a}^{\rm top}$ and a_r:

$$\ddot{a} = (\breve{a}^{\rm top} - \hat{a}^p_{\rm sat})\left(\frac{a_r}{a_r + a_s}\right). \tag{80}$$

Some of the localized rain and snow fluxes within the precipitation area ($\breve{F}^{\rm top}_R \equiv F^{\rm top}_R/\breve{a}^{\rm top}$ and $\breve{F}^{\rm top}_S \equiv F^{\rm top}_S/\breve{a}^{\rm top}$) falling into $\ddot{a}$ are evaporated or sublimated at the rates of

$$\ddot{E}_R = k_{e,R}(1 - \ddot{q}_v/\tilde{q}_s)\sqrt{\breve{F}^{\rm top}_R},$$
$$\ddot{E}_S = k_{e,S}(1 - \ddot{q}_v/\tilde{q}_s)\sqrt{\breve{F}^{\rm top}_S}, \tag{81}$$

where $\ddot{q}_v$ is the water vapor specific humidity within $\ddot{a}$ and $\tilde{q}_s$ is the saturation specific humidity of the environment in which temperature is assumed to be uniform. From $\tilde{q}_v$ and the normalized saturated stratus fraction $a^*_s = a_s/(1 - \sum_i \hat{a}^i)$ (note that CAM5 assumes $\hat{a}$ is horizonally nonoverlapped with a_s; see Park et al. 2014), we compute $\ddot{q}_v = (\tilde{q}_v - a^*_s\tilde{q}_s)/(1 - a^*_s)$. As long as $a^*_s(\widetilde{\rm RH}) < \widetilde{\rm RH}$, where $\widetilde{\rm RH}$ is the environmental relative humidity, $\ddot{q}_v$ is guaranteed to be positive (Park et al. 2014). Similar constraints imposed on the evaporation rate within the downdraft are imposed on the final $\ddot{E}_R$ and $\ddot{E}_S$.

The grid-mean tendency of $\phi = q_v, q_t, \theta_c$ due to the evaporation of convective precipitation within the environment is

$$\left(\tilde{a}\frac{\partial\tilde{q}_t}{\partial t}\right)_{\rm evp} = \left(\tilde{a}\frac{\partial\tilde{q}_v}{\partial t}\right)_{\rm evp} = \sum_i \ddot{a}^i(\ddot{E}^i_R + \ddot{E}^i_S) \quad \text{and} \tag{82}$$

$$\left(\tilde{a}\frac{\partial\tilde{\theta}_c}{\partial t}\right)_{\rm evp} = -\left(\frac{1}{C_p\pi}\right)\sum_i (L_v\ddot{a}^i\ddot{E}^i_R + L_s\ddot{a}^i\ddot{E}^i_S), \tag{83}$$

and the corresponding tendency for the environmental tracer is

$$\left(\tilde{a}\frac{\partial\tilde{\xi}}{\partial t}\right)_{\rm evp} = \sum_i \left(\tilde{a}\frac{\partial\tilde{q}_v}{\partial t}\right)^i_{\rm evp}\left(\frac{F^i_\xi}{F^i_R + F^i_S}\right). \tag{84}$$

The precipitation area at the base interface $\breve{a}^{\rm bot}$ that is used as $\breve{a}^{\rm top}$ in the layer below is

$$\breve{a}^{\rm bot} = \begin{cases} \breve{a}^{\rm top} + \hat{a}_{\rm prep} - \hat{a}^p_{\rm prep}, & \text{if} \quad \breve{F}^{\rm top}_R + \breve{F}^{\rm top}_S > (\Delta p/g)(\ddot{E}_R + \ddot{E}_S), \\ \breve{a}^{\rm top} - \ddot{a} + \hat{a}_{\rm prep} - \hat{a}^p_{\rm prep}, & \text{if} \quad \breve{F}^{\rm top}_R + \breve{F}^{\rm top}_S \le (\Delta p/g)(\ddot{E}_R + \ddot{E}_S), \end{cases} \tag{85}$$

where $\hat{a}_{\rm prep}$ is a precipitating $\hat{a}$ ($\hat{a}_{\rm prep} = \hat{a}$ if $P_R + P_S > 0$ but $\hat{a}_{\rm prep} = 0$ if $P_R + P_S = 0$) at the layer midpoint and $\hat{a}^p_{\rm prep}$ is the overlapping area between $\breve{a}^{\rm top}$ and $\hat{a}_{\rm prep}$, computed in a similar way as $\hat{a}^p_{\rm sat}$. By neglecting the horizontal drift of the rain and snow during fall, the location of the center of $\breve{a}^{\rm bot}$ at the base interface is

$$(\breve{x}^{\rm bot}, \breve{y}^{\rm bot}) = \frac{(\breve{x}^{\rm top}, \breve{y}^{\rm top})[F^{\rm top}_R + F^{\rm top}_S - (E_R + E_S)(\Delta p/g)] + (\hat{x}, \hat{y})(P_R + P_S)(\Delta p/g)}{F^{\rm top}_R + F^{\rm top}_S - (E_R + E_S)(\Delta p/g) + (P_R + P_S)(\Delta p/g)}, \tag{86}$$

where $E_R = \ddot{a}\ddot{E}_R$ and $E_S = \ddot{a}\ddot{E}_S$ are the grid-mean evaporation rates of the convective rain and snow within the environment. UNICON consecutively calculates Eqs. (80)–(86) from the updraft top to the lowest model layer and, from the independent precipitation approximation, Eqs. (80), (81), (85), and (86) are computed for individual convective updraft segment i.

2) SNOW MELTING

If $\tilde{T} > 273.15\,\mathrm{K}$, the convective snow flux falling into the top interface of the current layer and the new convective snow generated within the current layer are converted into rain. The energy necessary to melt the snow is provided by the environment. The resulting grid-mean snow melting tendency is

$$\left(\tilde{a}\frac{\partial\tilde{\theta}_c}{\partial t}\right)_{\mathrm{mlt}} = \begin{cases} -\left(\dfrac{1}{C_p\pi}\right)(L_s - L_v)\dfrac{g}{\Delta p}\displaystyle\sum_i F_S^{\mathrm{bot},i}, & \text{if} \quad \tilde{T} \geq 273.15\,\mathrm{K}, \\ 0, & \text{if} \quad \tilde{T} < 273.15\,\mathrm{K}, \end{cases} \tag{87}$$

where F_S^{bot} is the convective snow flux at the base interface of an individual layer. Snow melting only influences $\phi = \tilde{\theta}_c$ without changing the other scalars.

3) DISSIPATION HEATING OF MEAN KINETIC ENERGY

UNICON conserves the column-integrated horizontal momentum of the environment $I_u \equiv (1/g)\int_0^{p_s} \tilde{u}\,dp$ and $I_v \equiv (1/g)\int_0^{p_s} \tilde{v}\,dp$ but changes the column-integrated horizontal kinetic energy $I_{\mathrm{KE}} \equiv (1/g)\int_0^{p_s} [(\tilde{u}^2 + \tilde{v}^2)/2]\,dp$. CAM5 requires the conservation of the column-integrated total energy $I = I_{\mathrm{KE}} + I_s$, where $I_s \equiv (1/g)\int_0^{p_s} (C_p\tilde{T})\,dp$ is the column-integrated dry static energy per unit area. Using $\partial\tilde{u}/\partial t = g\partial F_u/\partial p$ and $\partial(\tilde{u}F_u)/\partial p = \tilde{u}\partial F_u/\partial p + F_u\partial\tilde{u}/\partial p$ (and similarly for the meridional momentum $\tilde{v}$), where F_u is the net vertical flux of the zonal momentum by convection, the conservation constraint of the column-integrated total energy can be written as $(\partial I_s/\partial t) = -(\partial I_{\mathrm{KE}}/\partial t) = \int_0^{p_s}(F_u\partial\tilde{u}/\partial p + F_v\partial\tilde{v}/\partial p)\,dp$. Following Boville and Bretherton (2003), UNICON satisfies this constraint by adding the dissipation heating $D \equiv g(F_u\partial\tilde{u}/\partial p + F_v\partial\tilde{v}/\partial p)$ in each layer:

$$\left(\tilde{a}\frac{\partial\tilde{\theta}_c}{\partial t}\right)_{\mathrm{dis}} = \left(\frac{g}{C_p\pi}\right)(F_u\partial\tilde{u}/\partial p + F_v\partial\tilde{v}/\partial p), \tag{88}$$

where D is not necessarily positive since convective momentum transport can be countergradient.

3. Summary and discussion

To further improve our understanding of observed convection, the author developed a unified convection scheme, called UNICON. Technically, UNICON is a relative subgrid vertical transport scheme by nonlocal asymmetric turbulent eddies (Fig. 1b), since, at any height, the thermodynamic properties of the convective plumes are the result of complex processes integrated from the origination level to the current height (i.e., nonlocal), not something that can be parameterized by the local grid-mean scalars at a single height, and the anomalous properties of convective updrafts (or downdrafts) relative to the grid-mean value are different from those of compensating subsidence (or upwelling) regions (i.e., asymmetric).

UNICON launches multiple convective updraft plumes from the surface and diagnoses the vertical profiles of the macrophysics (fractional area, plume radius, and number density) as well as the microphysics (production and evaporation rates of convective precipitation) and the dynamics (mass flux and vertical velocity) of multiple convective updraft and downdraft plumes (Fig. 3). UNICON simulates all dry–moist, forced–free and, shallow–deep convection within a single framework in a seamless, consistent, and unified way. Except for the evaporative enhancement of the mixing rate in a saturated cumulus updraft, no difference exists between the treatment of dry and moist convection. Dynamic treatment of various convective downdrafts allows UNICON to simulate both forced and free convection in a consistent way without using a separate penetrative entrainment closure at the cumulus top. Owing to the prognostic treatment of the subgrid cold pool and mesoscale organized flow, and its feedback on convective updrafts (Fig. 6), UNICON—a quasi-conserved diagnostic plume model—carries the convective plume memory across the model time steps and simulates both shallow and deep convection in a seamless and unified way without relying on any equilibrium assumptions, such as CAPE and CIN closures.

Because of the increase in computing power and societal demands to provide detailed regional information on future climate change, the future GCMs will be required to run at much higher horizontal resolution

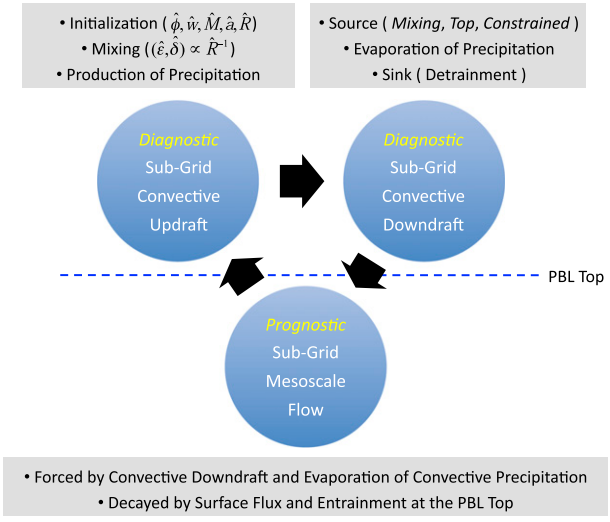

FIG. 6. Interaction among the three major components parameterized by UNICON. Convective downdrafts are generated from convective updrafts in any layers below the cumulus top in three different forms (mixing, top, and constrained). When forced by enough evaporation of convective precipitation, a convective downdraft can penetrate down into the PBL, generating subgrid cold pools and mesoscale organized flow within the PBL. The properties of the source updraft at the surface and mixing environmental air within and above the PBL are modulated by subgrid mesoscale organized flow. Both convective updraft and downdraft plumes are diagnostic without storage, so that their internal thermodynamic properties are not part of the prognosed grid-mean quantities. This lack of convective plume memory between the model time steps is complemented by the prognostic subgrid cold pools and mesoscale organized flow forced by convective downdrafts and evaporation of convective precipitation, which is used to reconstruct convective updraft plumes at the subsequent time step. See the text for more details.

($G_{\text{future}} \approx 10\,\text{km} \times 10\,\text{km}$) than now ($G_{\text{current}} \approx 100\,\text{km} \times 100\,\text{km}$). One of the biggest challenges is how to reduce the sensitivity of the combined advective–convective vertical transport to G, both in theoretical and practical aspects. The remainder of this section discusses whether UNICON meets the sufficient and necessary conditions to be scale adaptive as outlined in section 1.

The first condition is that a convection scheme simulates relative subgrid motion with respect to the resolved grid-mean flow, so that a seamless exclusive partitioning of the observed convection into the simulated advection–convection processes occurs over a wide range of G. UNICON is constructed to simulate the relative mass fluxes ($\hat{M}$, $\check{M}$) and the relative vertical velocities ($\hat{w}$, $\check{w}$). If $\pi\hat{R}^2_{\text{obs}} \ll G \approx \pi R^2_{\text{cs,obs}}$ (Fig. 2a), the observed convective updraft is solely simulated by the subgrid convective updraft parameterized by UNICON. However, if $G \to \pi\hat{R}^2_{\text{obs}}$ and so $\overline{w} \to \hat{w}_{\text{obs}}$, the grid-scale advection scheme takes the role of simulating the observed convective updraft (Fig. 2b). In the limiting case where $G < \pi\hat{R}^2_{\text{obs}}$ entirely resides within the homogeneous observed cumulus region (Fig. 2c), the grid-scale advection scheme solely simulates the observed convective updrafts, and in order to be scale adaptive, UNICON-simulated subgrid convective transport should be zero. Then, how does UNICON achieve this asymptotic behavior required to be scale adaptive? In the case of Fig. 2c, the mean environmental profile follows a saturated moist adiabat, so that the buoyancy of the parameterized convective updraft $\hat{B} = (g/\overline{\theta}_v)(1-\hat{a})(\hat{\theta}_v - \tilde{\theta}_v)$ is zero, leading to $\hat{w} \to 0$ by the entrainment dilution. In order to satisfy the consistency relationship of $0 \le \hat{a} \le \hat{A}_{\max} \ll 1$, where $\rho\hat{a} = \hat{M}/\hat{w}$, UNICON detrains all $\hat{M}$ (i.e., the source of the constrained downdraft) resulting in $\hat{M} \to 0$. In the opposite case of Fig. 2f where the $\tilde{\theta}_v$ profile is stable owing to the compensating subsidence, subgrid convective activity will be suppressed. Conceptually, the updraft plume radius simulated by UNICON is the radius of the upward portion of subgrid asymmetric turbulent eddies ($\pi\hat{R}^2 \le G\hat{A}_{\max}$), not the radius of the observed convective updraft. Thus, if $G \to 0$, $\hat{R} \to 0$ and $\hat{\epsilon}_o \to \infty$, so that convective updrafts are instantaneously homogenized to the environmental properties after being launched from the surface, resulting in zero subgrid convective flux.

One of the conceptual foundations of UNICON is that regardless of the size and the location of G relative to $\pi\hat{R}^2_{\text{obs}}$ and $\pi R^2_{\text{cs,obs}}$, the fractional area of the parameterized relative subgrid convective updraft is sufficiently small; that is, $\hat{A} = \sum_i \hat{a}^i \le \hat{A}_{\max} \ll 1$ (in the default, $\hat{A}_{\max}$ is set to 0.1), which is an alternative interpretation of the diagnostic plume approximation. This view is consistent with the fact that when $G \ll \pi R^2_{\text{cs,obs}}$, most of the observed convective updraft is simulated by the grid-scale advection scheme, so that the observed cumulus is defined mostly as the grid-scale prognostic stratus instead of the subgrid diagnostic cumulus in the GCM. This brings an additional merit since the treatment of the cloud macro–microphysics and the radiative properties of GCM-simulated stratus is more sophisticated than the cumulus. However, in the case in which $G \ll \pi R^2_{\text{cs,obs}}$, our conceptual view naturally breaks the analogy between the observed convective updraft and the parameterized subgrid convective updraft, which is valid only when $G \approx \pi R^2_{\text{cs,obs}}$. An alternative way to maintain such an analogy is to set $\hat{A}_{\max} = 1$, so that the observed convective updraft in Figs. 2b and 2c is defined as the subgrid convective updraft with $\hat{A} \to 1$. While this approach seems to ensure scale adaptivity in terms of the subgrid convective flux because of the rapid reduction of $\hat{B}$ as $\hat{a}$ increases [note that $(1-\hat{a})$ is multiplied in the definition of $\hat{B}$], its physical validity is questionable in the framework of the diagnostic plume model in which the internal properties of a convective plume are not

prognosed. For example, in the case of Fig. 2c, we will have trouble defining the prognostic grid-mean thermodynamic scalars. It is likely that this alternative approach with $\hat{A}_{\max} = 1$ should be used in conjunction with a prognostic plume model. Finally, we note that conventional deep convection schemes designed to simulate the observed convection have a conceptual deadlock in obtaining scale adaptivity owing to the use of quasi-equilibrium assumption between the grid-scale destabilization and the subgrid convective stabilization, which is valid only when $G \approx \pi R^2_{\text{cs,obs}}$ (since the stabilization by convection in nature occurs in the compensating subsidence region) and the time scale of the observed convection is shorter than the model integration time step.

The second condition for scale adaptivity is that the relative subgrid motion parameterized by the convection scheme is completely separated from the relative subgrid motion parameterized by the PBL scheme. Since UNICON is a subgrid vertical transport scheme by nonlocal asymmetric turbulent eddies, this requirement can be satisfied if the PBL scheme is designed to simulate local symmetric turbulent eddies. In CAM5, the moist PBL scheme computes turbulent flux using a first-order K-diffusion theory without a nonlocal transport term; that is, $\overline{w'\phi'} = -K\partial\overline{\phi}/\partial z$, where $K = l\sqrt{e}S$ is an eddy diffusivity with a turbulent length scale l, e is TKE, and S is a stability parameter, which is a function of the local Richardson number. This formulation is derived from the symmetric turbulence assumption that the anomalous properties of turbulent updraft eddies are identical to those of turbulent downdraft eddies (i.e., $\hat{a} = \check{a} = 0.5$, $|\hat{w}_o - \overline{w}| = |\check{w}_o - \overline{w}|$, $|\hat{\phi} - \overline{\phi}| = |\check{\phi} - \overline{\phi}|$) solely deducible from the vertical gradient of local grid-mean scalars. It is clear that turbulent eddies simulated by the CAM5 PBL scheme are local symmetric, and well separated from nonlocal asymmetric turbulent eddies simulated by UNICON (Fig. 1b).

The third condition is that the PBL and convection schemes should be able to parameterize the entire relative subgrid motion together. This is a challenging issue. Since all convective updrafts rise from the surface, currently, UNICON does not simulate elevated convection. While UNICON parameterizes the feedback effects on the convective updrafts by the internal mesoscale organized flow driven by the evaporation of convective precipitation and accompanying convective downdrafts, the contribution of the other external sources of the mesoscale organized flows (e.g., subgrid orography, subgrid land–sea–ice contrasts) are not included. In addition, vertical fluxes from the subgrid mesoscale flows themselves (e.g., fluxes driven by the bulk mesoscale flow within the PBL and the enhancement of surface fluxes by organized surface winds) have not been activated yet. UNICON provides a flexible framework to implement these processes in the future.

Acknowledgments. The author expresses his deepest thanks to the late Prof. Conway B. Leovy at the University of Washington, the author's Ph.D. advisor and lifetime mentor, who has continuously encouraged the author not to be afraid of challenging himself and learning from trial and error. Without his encouragement, the author could not have finished this work. Great thanks also go to Joe Tribbia at NCAR, who helped the author to concentrate on this work during the last 5 years; Brian Mapes at the University of Miami, who provided an important clue on the parameterization of mesoscale convective organization; Minoru Chikira at JAMSTEC, who provided a thorough and insightful review on the initial draft; and anonymous reviewers and the editor. The greatest thanks go to God and the author's family. The author is supported by the National Science Foundation. Part of this work was supported by the NOAA MAPP program under Grant NA10OAR4310261; the Regional and Global Climate Modeling Program of the U.S. Department of Energy's (DOE) Office of Science Cooperative Agreement DE-FC02-97ER62402; and DOE-NSF EaSM project under Grant DE-SC0006690.

APPENDIX A

Profile Reconstruction

Following BMG04 and PB09, UNICON uses a profile reconstruction technique to compute the internal slope of individual environmental scalars within each grid layer. Profile reconstruction conserves the layer-mean scalar and reduces the sensitivity of the convection scheme to vertical resolution, which is particularly beneficial for GCMs with coarse vertical grids. For each environmental scalar $\tilde{\phi}$, we compute an upper slope $\tilde{\gamma}^{\text{up}}(k) \equiv [\tilde{\phi}(k+1) - \tilde{\phi}(k)]/[p(k+1) - p(k)]$ and a lower slope $\tilde{\gamma}^{\text{dn}}(k) \equiv [\tilde{\phi}(k) - \tilde{\phi}(k-1)]/[p(k) - p(k-1)]$, where k is a layer index increasing upward from the lowest model layer, $k = 1$. Then, the slope with a smaller absolute value is taken as the reconstructed slope $\tilde{\gamma}(k)$. If $\tilde{\gamma}^{\text{up}}(k)$ and $\tilde{\gamma}^{\text{dn}}(k)$ have different signs, $\tilde{\gamma}(k)$ is set to zero. In the lowest model layer, $\tilde{\gamma} = \tilde{\gamma}^{\text{up}}$, but in the highest model layer, $\tilde{\gamma} = \tilde{\gamma}^{\text{dn}}$. We perform the same profile reconstruction on each of $\phi = q_t, \theta_c, u, v, \xi$. Then, $\tilde{\phi}^{\text{top}}$ and $\tilde{\phi}^{\text{bot}}$ are computed at the top and bottom interfaces of each layer, which inevitably causes discontinuity in the reconstructed $\tilde{\phi}$ profile at the model interfaces as shown in Fig. 4a. For consistency, the identical profile reconstruction is used in the subgrid local symmetric turbulence scheme in CAM5 (Bretherton and Park 2009).

APPENDIX B

Saturation Mixing Fraction χ_s and Critical Mixing Fraction χ_c

Updraft buoyancy sorting is performed at the base interface of each layer. The mixture within $0 \le \chi \le \chi_c$ has a buoyancy and vertical velocity great enough to rise over a critical distance $l_c = r_c \hat{z}_{\rm top}(t - \Delta t)$ from the base interface (Fig. 4b), where $\hat{z}_{\rm top}(t - \Delta t)$ is the mean top height of the precedent updraft plumes weighted by the updraft mass flux at the surface. First, we compute a saturation mixing fraction χ_s at which the mixture is saturated without condensate:

$$\chi_s = \frac{\hat{X}}{\hat{X} - \tilde{X}_u}, \quad \text{if} \quad \hat{X}\tilde{X}_u < 0, \tag{B1}$$

where $\hat{X}$ and $\tilde{X}_u$ are the saturation excesses of the convective updraft and the mixing environmental air, respectively, computed as $\hat{X} = \hat{q}_t - q_s(\hat{T}_c)$ and $\tilde{X}_u = \tilde{q}_{t,u} - q_s(\tilde{T}_{c,u})$ with condensate temperature $\hat{T}_c = \pi\hat{\theta}_c$ and $\tilde{T}_{c,u} = \pi\tilde{\theta}_{c,u}$, where q_s is saturation specific humidity and θ_c is condensate potential temperature defined in section 2a. The above equation is obtained by approximating $q_s[(1-\chi_s)\hat{T}_c + \chi_s\tilde{T}_{c,u}] \approx (1-\chi_s)q_s(\hat{T}_c) + \chi_s q_s(\tilde{T}_{c,u})$. If $\hat{X} > \tilde{X}_u$, the unsaturated segment is $\chi_s < \chi < 1$, while if $\hat{X} < \tilde{X}_u$, the unsaturated segment is $0 < \chi < \chi_s$. If $\hat{X}\tilde{X}_u \ge 0$, the mixture is totally saturated or unsaturated for $0 < \chi < 1$. Following BMG04 and PB09, the $\theta_v(\chi)$ of the mixture is assumed to be a piecewise linear function of χ between $0 \le \chi < \chi_s$ and $\chi_s \le \chi \le 1$. We compute χ_c by solving the following quadratic equation obtained by integrating Eq. (27) with $\hat{\epsilon} = \hat{\delta} = 0$, $\hat{w}^{\rm bot} \to w(\chi) = (1-\chi)\hat{w}^{\rm bot} + \chi\tilde{w}_u^{\rm bot}$ with $\tilde{w}_u^{\rm bot} = 0$, and $\hat{w}^{\rm top} = 0$ after a vertical displacement of l_c, assuming $\hat{B}$ does not change with height for simplicity:

$$A\chi_c^2 + B\chi_c + C = 0, \tag{B2}$$

where

$$A = (\hat{w}^{\rm bot})^2,$$

$$B = 2a(\hat{R})gl_c\left(\frac{\theta_{v,1} - \theta_{v,0}}{\tilde{\theta}_v}\right) - 2(\hat{w}^{\rm bot})^2, \quad \text{and}$$

$$C = 2a(\hat{R})gl_c\left(\frac{\theta_{v,0} - \tilde{\theta}_v}{\tilde{\theta}_v}\right) + (\hat{w}^{\rm bot})^2,$$

and if the mesoscale organized flow exists within the PBL, we use $w(\chi) = (1-\chi)\hat{w}^{\rm bot} + \chi\Delta w_\Omega$ [here, Δw_Ω is from Eq. (74)], which results in the use of $A = (\hat{w}^{\rm bot} - \Delta w_\Omega)^2$ and $\hat{w}^{\rm bot}(\hat{w}^{\rm bot} - \Delta w_\Omega)$ instead of $(\hat{w}^{\rm bot})^2$ on the rhs of the above B. If $\hat{X}\tilde{X}_u > 0$, we solve Eq. (B2) with $\theta_{v,0} = \hat{\theta}_v$ and $\theta_{v,1} = \tilde{\theta}_{v,u}$. If $\hat{X}\tilde{X}_u < 0$, Eq. (B2) is solved twice for the $0 \le \chi \le \chi_s$ segment with $\theta_{v,0} = \hat{\theta}_v$ and $\theta_{v,1} = (1 - 1/\chi_s)\hat{\theta}_v + (1/\chi_s)\theta_v(\chi_s)$ and the $\chi_s < \chi \le 1$ segment with $\theta_{v,0} = [\chi_s/(\chi_s - 1)]\tilde{\theta}_{v,u} + [1/(1-\chi_s)]\theta_v(\chi_s)$ and $\theta_{v,1} = \tilde{\theta}_{v,u}$, respectively.

APPENDIX C

Formulation of Cold Pools within the PBL

The goal is to derive a complete set of budget equations in a_U from which convective updrafts rise and in a_D into which convective downdrafts sink at the PBL top (Fig. 5). While the details of the formulation differ, Grandpeix and Lafore (2010) explored a conceptually similar approach. Consider a GCM grid containing several sets of a_D^l—cold pools—within the PBL. The cold pool within the lth category is generated by the convective downdrafts exclusively sinking down into the lth cold pool. We assume there also exist other convective downdrafts that fall exclusively into a_U or uniformly over the entire grid. An individual convective updraft (downdraft) induces compensating subsidence (upwelling). For simplicity, the vertical variation of environmental thermodynamic scalars within the PBL is neglected, and only the bulk horizontal heterogeneity between a_U and a_D and within $a_D = \sum_l a_D^l$ is considered. Conceptually, the grid-mean tendency of any scalar ϕ averaged over the PBL can be induced by grid-scale horizontal advection; subgrid turbulent flux at the PBL top, by convective updrafts rising out of the PBL and convective downdrafts sinking down into the PBL, and by other types of turbulent eddies; subgrid turbulent flux at the surface; sources within the PBL; and the other nonturbulent physical processes. Assuming $\overline{\phi} \approx \tilde{\phi}$ from $\hat{A} \ll 1$ and $\check{a} \to 0$ that UNICON is based on, this conceptual budget can be formulated as follows:

$$\begin{aligned}\frac{\partial \phi_{\rm PBL}}{\partial t} = &-U_{\rm PBL}\frac{\partial \phi_{\rm PBL}}{\partial x} - V_{\rm PBL}\frac{\partial \phi_{\rm PBL}}{\partial y}\\ &- \left(\frac{g}{\Delta p_h}\right)\left\{\sum_i \hat{M}_h^i(\hat{\phi}^i - \phi_{\rm PBL}) - \sum_j\left[\sum_l \check{M}_{D,h}^{j,l}(\check{\phi}_{D,h}^{j,l} - \phi_{\rm PBL}) + \check{M}_{U,h}^{j}(\check{\phi}_{U,h}^{j} - \phi_{\rm PBL})\right]\right\}\\ &+ \left(\frac{g}{\Delta p_h}\right)\left[\sum_j \check{M}_{G,h}^{j}(\check{\phi}_{G,h}^{j} - \phi_{\rm PBL}) + \rho_h W_{e,h}(\phi_f - \phi_{\rm PBL}) + (\rho\overline{w'\phi'})_s\right] + \langle\overline{S}\rangle_0^h + \langle\overline{F}_\phi\rangle_0^h,\end{aligned} \tag{C1}$$

where $\phi = q_t, \theta_c, u, v, \xi$; the superscripts i and j are the indices denoting individual convective updrafts and downdrafts, respectively; the subscript h denotes the value at the PBL top; the bracket $\langle\cdot\rangle_0^h$ is the vertical average over the PBL depth with 0 and h denoting the surface and the PBL-top height, respectively; $\phi_{\rm PBL} \equiv \langle\tilde{\phi}\rangle_0^h$ is the environmental scalar averaged over the PBL; $U_{\rm PBL} \equiv \langle\tilde{u}\rangle_0^h$ and $V_{\rm PBL} \equiv \langle\tilde{v}\rangle_0^h$ are the environmental zonal and meridional winds averaged over the PBL; $\Delta p_h > 0$ is the depth of the PBL; $(\check{M}_U, \check{M}_D, \check{M}_G)$ and $(\check{\phi}_U, \check{\phi}_D, \check{\phi}_G)$ denote the mass fluxes and the scalars of the convective downdrafts that sink exclusively into a_U and a_D and over the entire grid, respectively; ϕ_f is the mean scalar in the free atmosphere just above the PBL; $W_{e,h}$ is an entrainment rate at the PBL top given from the separate subgrid vertical transport scheme by local symmetric turbulent eddies; $(\rho\overline{w'\phi'})_s$ is the upward turbulent flux at the surface; $\langle\overline{S}\rangle_0^h = a_U\langle S_U\rangle_0^h + \sum_l a_D^l\langle S_D^l\rangle_0^h$ is the grid-mean source averaged over the PBL, with S_U and S_D^l denoting the sources within a_U and a_D^l, respectively; and $\langle\overline{F}_\phi\rangle_0^h$ is a sum of all nonconvective grid-mean forcings averaged over the PBL except the ones by the grid-scale horizontal advection and the PBL schemes (e.g., stratus macro–microphysics, radiation, etc.), which is assumed to be horizontally uniform within the grid, for simplicity. We also assume that $W_{e,h}$ is horizontally uniform within the grid. Note that all the mass fluxes are relative mass fluxes, and the downdraft mass flux is regarded as a positive quantity ($\check{M}^j > 0$) for the cold pool formulation in this section. The convective downdraft that sinks exclusively down into a_D (i.e., $\check{M}_{D,h}$, $\check{\phi}_{D,h}$) is defined as the mixing downdraft that has originated from above the PBL top, is accompanied by nonzero precipitation flux at the PBL-top interface, and can sink all the way down to the lowest model interface above the surface. The scalar content equations in each a_U and a_D^l region are given by

$$\begin{aligned}\frac{\partial}{\partial t}(a_U\phi_U) = &-U_{\rm PBL}\frac{\partial}{\partial x}(a_U\phi_U) - V_{\rm PBL}\frac{\partial}{\partial y}(a_U\phi_U)\\ &+\sum_l(\delta_c^l\phi_D^l - \epsilon_c^l\phi_U) - \left(\frac{g}{\Delta p_h}\right)\left[\sum_i \hat{M}_h^i(\hat{\phi}^i - a_U\phi_U) + (a_U\phi_U)\sum_j\sum_l \check{M}_{D,h}^{j,l} - \sum_j \check{M}_{U,h}^j(\check{\phi}_{U,h}^j - a_U\phi_U)\right]\\ &+a_U\left(\frac{g}{\Delta p_h}\right)\left[\sum_j \check{M}_{G,h}^j(\check{\phi}_{G,h}^j - \phi_U) + \rho_h W_{e,h}(\phi_f - \phi_U) + (\rho\overline{w'\phi'})_{s,U}\right] + a_U\langle S_U\rangle_0^h + a_U\langle\overline{F}_\phi\rangle_0^h \quad \text{and}\end{aligned} \tag{C2}$$

$$\begin{aligned}\frac{\partial}{\partial t}(a_D^l\phi_D^l) = &-U_{\rm PBL}\frac{\partial}{\partial x}(a_D^l\phi_D^l) - V_{\rm PBL}\frac{\partial}{\partial y}(a_D^l\phi_D^l) + (\epsilon_c^l\phi_U - \delta_c^l\phi_D^l)\\ &+\left(\frac{g}{\Delta p_h}\right)\left\{(a_D^l\phi_D^l)\left(\sum_i \hat{M}_h^i - \sum_j\sum_{m\neq l}\check{M}_{D,h}^{j,m} - \sum_j \check{M}_{U,h}^j\right) + \sum_j \check{M}_{D,h}^{j,l}(\check{\phi}_{D,h}^{j,l} - a_D^l\phi_D^l)\right\}\\ &+a_D^l\left(\frac{g}{\Delta p_h}\right)\left[\sum_j \check{M}_{G,h}^j(\check{\phi}_{G,h}^j - \phi_D^l) + \rho_h W_{e,h}(\phi_f - \phi_D^l) + (\rho\overline{w'\phi'})_{s,D}^l\right] + a_D^l\langle S_D^l\rangle_0^h + a_D^l\langle\overline{F}_\phi\rangle_0^h,\end{aligned} \tag{C3}$$

where ϕ_U and ϕ_D^l are the environmental scalars averaged over the PBL within a_U and a_D^l, respectively; ϵ_c and δ_c denote the lateral entrainment and detrainment rates between a_D and a_U, respectively (here, subscript c stands for the cold pool); and $\partial\phi_{\rm PBL}/\partial t = \partial(a_U\phi_U)/\partial t + \partial(\sum_l a_D^l\phi_D^l)/\partial t$. The corresponding mass budget equations are

$$\frac{\partial a_U}{\partial t} = -U_{\rm PBL}\frac{\partial a_U}{\partial x} - V_{\rm PBL}\frac{\partial a_U}{\partial y} + \sum_l(\delta_c^l - \epsilon_c^l) - \left(\frac{g}{\Delta p_h}\right)\left[\left(\sum_i \hat{M}_h^i - \sum_j \check{M}_{U,h}^j\right)\left(\sum_l a_D^l\right) + a_U\sum_j\sum_l \check{M}_{D,h}^{j,l}\right] \quad \text{and} \tag{C4}$$

$$\frac{\partial a_D^l}{\partial t} = -U_{\rm PBL}\frac{\partial a_D^l}{\partial x} - V_{\rm PBL}\frac{\partial a_D^l}{\partial y} + (\epsilon_c^l - \delta_c^l) + \left(\frac{g}{\Delta p_h}\right)\left[a_D^l\left(\sum_i \hat{M}_h^i - \sum_j \check{M}_{U,h}^j\right) + (1-a_D^l)\sum_j \check{M}_{D,h}^{j,l} - a_D^l\sum_j\sum_{m\neq l}\check{M}_{D,h}^{j,m}\right], \tag{C5}$$

which satisfies $\partial a_U/\partial t + \partial(\sum_l a_D^l)/\partial t = 0$. Using Eqs. (C2)–(C5), we can derive the following scalar budget equations for ϕ_U and ϕ_D^l:

$$\frac{\partial \phi_U}{\partial t} = -U_{\rm PBL}\frac{\partial \phi_U}{\partial x} - V_{\rm PBL}\frac{\partial \phi_U}{\partial y} + \left(\frac{1}{a_U}\right)\sum_l \delta_c^l(\phi_D^l - \phi_U) + \left(\frac{g}{\Delta p_h}\right)\left(\frac{1}{a_U}\right)\left[\sum_j \check{M}_{U,h}^j(\check{\phi}_{U,h}^j - \phi_U) - \sum_i \hat{M}_h^i(\hat{\phi}_h^i - \phi_U)\right] + \left(\frac{g}{\Delta p_h}\right)\left[\sum_j \check{M}_{G,h}^j(\check{\phi}_{G,h}^j - \phi_U) + \rho_h W_{e,h}(\phi_f - \phi_U) + (\rho\overline{w'\phi'})_{s,U}\right] + \langle S_U\rangle_0^h + \langle \overline{F}_\phi\rangle_0^h, \quad \text{and} \tag{C6}$$

$$\frac{\partial \phi_D^l}{\partial t} = -U_{\rm PBL}\frac{\partial \phi_D^l}{\partial x} - V_{\rm PBL}\frac{\partial \phi_D^l}{\partial y} + \left(\frac{1}{a_D^l}\right)\epsilon_c^l(\phi_U - \phi_D^l) + \left(\frac{g}{\Delta p_h}\right)\left(\frac{1}{a_D^l}\right)\sum_j \check{M}_{D,h}^{j,l}(\check{\phi}_{D,h}^{j,l} - \phi_D^l) + \left(\frac{g}{\Delta p_h}\right)\left[\sum_j \check{M}_{G,h}^j(\check{\phi}_{G,h}^j - \phi_D) + \rho_h W_{e,h}(\phi_f - \phi_D^l) + (\rho\overline{w'\phi'})_{s,D}^l\right] + \langle S_D^l\rangle_0^h + \langle \overline{F}_\phi\rangle_0^h. \tag{C7}$$

For simplicity, we assume that only one type of a_D^l exists within the PBL. Then, $a_D^l = a_D = 1 - a_U$ and all terms with $\sum_{m\neq l}$ become zero. We use the bulk formula for surface flux computation $(\rho\overline{w'\phi'})_s = \rho_s C_d V_s(\phi_s - \phi_{\rm PBL}) = a_U(\rho\overline{w'\phi'})_{s,U} + a_D(\rho\overline{w'\phi'})_{s,D}$ by assuming that the surface exchange coefficient C_d and surface wind speed V_s are horizontally uniform within the grid.

In order to complete the formulation of the cold pool and its feedback on the convective updrafts, we should compute the time evolution of $\Delta\phi_U \equiv \phi_U - \phi_{\rm PBL}$ and, accordingly, $\langle S_U - \overline{S}\rangle_0^h$, the difference of the sources in the regions between a_U and the entire grid. Similar computation is necessary for $\Delta\phi_D \equiv \phi_D - \phi_{\rm PBL}$ and $\langle S_D - \overline{S}\rangle_0^h$. Assumed to be uniform over the grid, $\langle \overline{F}_\phi\rangle_0^h$ does not contribute to $\Delta\phi_U$ and $\Delta\phi_D$. In UNICON, sources can exist in five different components: convective updrafts ($\hat{M}$), convective downdrafts exclusively sinking into a_D ($\check{M}_D$), convective downdrafts exclusively sinking into a_U ($\check{M}_U$), convective downdrafts sinking uniformly over the grid ($\check{M}_G$), and finally the environment. Among these, the $\check{M}_G$ component does not contribute to $\langle S_U - \overline{S}\rangle_0^h$ and $\langle S_D - \overline{S}\rangle_0^h$, since $\check{M}_G$ is uniformly distributed over the grid. Thus,

$$S_U - \overline{S} = (S_U - \overline{S})_u + (S_U - \overline{S})_{d,D} + (S_U - \overline{S})_{d,U} + (S_U - \overline{S})_e, \quad \text{and} \tag{C8}$$

$$S_D - \overline{S} = (S_D - \overline{S})_u + (S_D - \overline{S})_{d,D} + (S_D - \overline{S})_{d,U} + (S_D - \overline{S})_e, \tag{C9}$$

where $(S_U - \overline{S})_u = (1/a_U)g\sum_i \hat{M}^i\hat{S}_\phi^i - g\sum_i \hat{M}^i\hat{S}_\phi^i = (a_D/a_U)g\sum_i \hat{M}^i\hat{S}_\phi^i$ and $(S_D - \overline{S})_u = -g\sum_i \hat{M}^i\hat{S}_\phi^i$ since $\hat{M}$ exists only within a_U; $(S_U - \overline{S})_{d,D} = -g\sum_j \check{M}_D^j\check{S}_{\phi,D}^j$ and $(S_D - \overline{S})_{d,D} = (1/a_D)g\sum_j \check{M}_D^j\check{S}_{\phi,D}^j - g\sum_j \check{M}_D^j\check{S}_{\phi,D}^j = (a_U/a_D)g\sum_j \check{M}_D^j\check{S}_{\phi,D}^j$ since $\check{M}_D$ exclusively sinks down into a_D; and $(S_U - \overline{S})_{d,U} = (1/a_U)g\sum_j \check{M}_U^j\check{S}_{\phi,U}^j - g\sum_j \check{M}_U^j\check{S}_{\phi,U}^j = (a_D/a_U)g\sum_j \check{M}_U^j\check{S}_{\phi,U}^j$ and $(S_D - \overline{S})_{d,U} = -g\sum_j \check{M}_U^j\check{S}_{\phi,U}^j$ since $\check{M}_U$ exclusively sinks down into a_U. As a result,

$$S_U - \overline{S} = \left(\frac{a_D}{a_U}\right)g\left(\sum_i \hat{M}^i\hat{S}_\phi^i + \sum_j \check{M}_U^j\check{S}_{\phi,U}^j\right) - g\sum_j \check{M}_D^j\check{S}_{\phi,D}^j + (S_U - \overline{S})_e \quad \text{and} \tag{C10}$$

$$S_D - \overline{S} = \left(\frac{a_U}{a_D}\right)g\sum_j \check{M}_D^j\check{S}_{\phi,D}^j - g\left(\sum_i \hat{M}^i\hat{S}_\phi^i + \sum_j \check{M}_U^j\check{S}_{\phi,U}^j\right) + (S_D - \overline{S})_e, \tag{C11}$$

where $\hat{S}_\phi$, $\check{S}_{\phi,D}$, and $\check{S}_{\phi,U}$ are computed in sections 2b(5) and 2c(3). The differential sources within the environment $[(S_U - \overline{S})_e, (S_D - \overline{S})_e]$ are from either the evaporation of convective precipitation or the melting of convective snow. In contrast to $\hat{M}$ and $\check{M}$, convective precipitation may fall into any areas of a_U and a_D: if it falls uniformly (or randomly) over the grid, then $(S_U - \overline{S})_e = 0$ and $(S_D - \overline{S})_e = 0$, while if it falls exclusively into a_D, then it becomes $(S_U - \overline{S})_e = -\tilde{a}(\partial\tilde{\phi}/\partial t)_s$ and $(S_D - \overline{S})_e = (a_U/a_D)\tilde{a}(\partial\tilde{\phi}/\partial t)_s$. In order to provide a general treatment, UNICON uses a specified overlapping parameter β between the area of convective precipitation (or evaporation of convective precipitation) and a_U. Then $(S_U - \overline{S})_e$ and $(S_D - \overline{S})_e$ are formulated as a function of β, as shown in Eqs. (65)–(69) with $(S_U - \overline{S})_e = S_{e,U} - \overline{S}_e$ and $(S_D - \overline{S})_e = S_{e,D} - \overline{S}_e$, respectively.

REFERENCES

Arakawa, A., and W. Schubert, 1974: Interaction of a cumulus cloud ensemble with the large-scale environment, Part I. *J. Atmos. Sci.,* **31,** 674–701, doi:10.1175/1520-0469(1974)031<0674:IOACCE>2.0.CO;2.

——, and C.-M. Wu, 2013: A unified representation of deep moist convection in numerical modeling of the atmosphere. Part I. *J. Atmos. Sci.,* **70,** 1977–1992, doi:10.1175/JAS-D-12-0330.1.

Bechtold, P., M. Köhler, T. Jung, F. Doblas-Reyes, M. Leutbecher, M. J. Rodwell, F. Vitart, and G. Balsamo, 2008: Advances in simulating atmospheric variability with the ECMWF model: From synoptic to decadal time-scales. *Quart. J. Roy. Meteor. Soc.,* **134,** 1337–1351, doi:10.1002/qj.289.

Boville, B. A., and C. S. Bretherton, 2003: Heating and kinetic energy dissipation in the ncar community atmosphere model. *J. Climate,* **16,** 3877–3887, doi:10.1175/1520-0442(2003)016<3877:HAKEDI>2.0.CO;2.

Bretherton, C. S., and S. Park, 2009: A new moist turbulence parameterization in the Community Atmosphere Model. *J. Climate,* **22,** 3422–3448, doi:10.1175/2008JCLI2556.1.

——, J. R. McCaa, and H. Grenier, 2004: A new parameterization for shallow cumulus convection and its application to marine subtropical cloud-topped boundary layers. Part I: Description and 1D results. *Mon. Wea. Rev.,* **132,** 864–882, doi:10.1175/1520-0493(2004)132<0864:ANPFSC>2.0.CO;2.

Chikira, M., and M. Sugiyama, 2010: A cumulus parameterization with state-dependent entrainment rate. Part I: Description and sensitivity to temperature and humidity profiles. *J. Atmos. Sci.,* **67,** 2171–2193, doi:10.1175/2010JAS3316.1.

——, and ——, 2013: Eastward-propagating intraseasonal oscillation represented by Chikira–Sugiyama cumulus parameterization. Part I: Comparison with observation and reanalysis. *J. Atmos. Sci.,* **70,** 3920–3939, doi:10.1175/JAS-D-13-034.1.

Dawe, J., and P. Austin, 2013: Direct entrainment and detrainment rate distributions of individual shallow cumulus clouds in an LES. *Atmos. Chem. Phys. Discuss.,* **13,** 5365–5410, doi:10.5194/acpd-13-5365-2013.

de Rooy, W. C., and A. P. Siebesma, 2010: Analytical expressions for entrainment and detrainment in cumulus convection. *Quart. J. Roy. Meteor. Soc.,* **136,** 1216–1227, doi:10.1002/qj.640.

Emanuel, K. A., 1981: A similarity theory for unsaturated downdrafts within clouds. *J. Atmos. Sci.,* **38,** 1541–1557, doi:10.1175/1520-0469(1981)038<1541:ASTFUD>2.0.CO;2.

——, 1991: A scheme for representing cumulus convection in large-scale models. *J. Atmos. Sci.,* **48,** 2313–2329, doi:10.1175/1520-0469(1991)048<2313:ASFRCC>2.0.CO;2.

Galperin, B., L. Kantha, S. Hassid, and A. Rosati, 1988: A quasi-equilibrium turbulent energy model for geophysical flows. *J. Atmos. Sci.,* **45,** 55–62, doi:10.1175/1520-0469(1988)045<0055:AQETEM>2.0.CO;2.

Grandpeix, J.-Y., and J.-P. Lafore, 2010: A density current parameterization coupled with Emanuel's convection scheme. Part I: The models. *J. Atmos. Sci.,* **67,** 881–897, doi:10.1175/2009JAS3044.1.

Gregory, D., 2001: Estimation of entrainment rate in simple models of convective clouds. *Quart. J. Roy. Meteor. Soc.,* **127,** 53–72, doi:10.1002/qj.49712757104.

——, R. Kershaw, and P. Inness, 1997: Parametrization of momentum transport by convection. II: Tests in single-column and general circulation models. *Quart. J. Roy. Meteor. Soc.,* **123,** 1153–1183, doi:10.1002/qj.49712354103.

Hahn, C. J., and S. G. Warren, 1999: Extended edited synoptic cloud reports from ships and land stations over the globe, 1952–1996. U.S. Department of Energy, Office of Biological and Environmental Research, Environmental Sciences Division Publ. 4913, ORNL/CDIAC-123, NDP-026C, 76 pp, doi:10.3334/CDIAC/cli.ndp026c.

Hohenegger, C., and C. S. Bretherton, 2011: Simulating deep convection with a shallow convection scheme. *Atmos. Chem. Phys.,* **11,** 10 389–10 406, doi:10.5194/acp-11-10389-2011.

Holtslag, A., and B. Boville, 1993: Local versus nonlocal boundary-layer diffusion in a global climate model. *J. Climate,* **6,** 1825–1842, doi:10.1175/1520-0442(1993)006<1825:LVNBLD>2.0.CO;2.

Kain, J. S., and J. M. Fritsch, 1990: A one-dimensional entraining/detraining plume model and its application in convective parameterization. *J. Atmos. Sci.,* **47,** 2784–2802, doi:10.1175/1520-0469(1990)047<2784:AODEPM>2.0.CO;2.

Kim, D., and Coauthors, 2009: Application of mjo simulation diagnostics to climate models. *J. Climate,* **22,** 6413–6436, doi:10.1175/2009JCLI3063.1.

Kuo, H.-L., 1965: On formation and intensification of tropical cyclones through latent heat release by cumulus convection. *J. Atmos. Sci.,* **22,** 40–63, doi:10.1175/1520-0469(1965)022<0040:OFAIOT>2.0.CO;2.

——, 1974: Further studies of the parameterization of the influence of cumulus convection on large-scale flow. *J. Atmos. Sci.,* **31,** 1232–1240, doi:10.1175/1520-0469(1974)031<1232:FSOTPO>2.0.CO;2.

Madden, R. A., and P. R. Julian, 1971: Detection of a 40–50 day oscillation in the zonal wind in the tropical Pacific. *J. Atmos. Sci.,* **28,** 702–708, doi:10.1175/1520-0469(1971)028<0702:DOADOI>2.0.CO;2.

Mapes, B., and R. Neale, 2011: Parameterizing convective organization to escape the entrainment dilemma. *J. Adv. Model. Earth Syst.,* **3,** M06004, doi:10.1029/2011MS000042.

Mellor, G. L., and T. Yamada, 1982: Development of a turbulence closure model for geophysical fluid problems. *Rev. Geophys.,* **20,** 851–875, doi:10.1029/RG020i004p00851.

Moncrieff, M. W., D. E. Waliser, M. J. Miller, M. A. Shapiro, G. R. Asrar, and J. Caughey, 2012: Multiscale convective organization and the YOTC virtual global field campaign. *Bull. Amer. Meteor. Soc.,* **93,** 1171–1187, doi:10.1175/BAMS-D-11-00233.1.

Monin, A., and A. Obukhov, 1954: Basic laws of turbulent mixing in the surface layer of the atmosphere. *Contrib. Geophys. Inst. Acad. Sci. USSR,* **151,** 163–187.

Neggers, R. A. J., A. P. Siebesma, and H. J. J. Jonker, 2002: A multiparcel model for shallow cumulus convection. *J. Atmos.*

Sci., **59,** 1655–1668, doi:10.1175/1520-0469(2002)059<1655:AMMFSC>2.0.CO;2.

Park, S., 2014: A unified convection scheme (UNICON). Part II: Simulation. *J. Atmos. Sci.,* **71,** 3931–3973, doi:10.1175/JAS-D-13-0234.1.

——, and C. B. Leovy, 2004: Marine low-cloud anomalies associated with ENSO. *J. Climate,* **17,** 3448–3469, doi:10.1175/1520-0442(2004)017<3448:MLAAWE>2.0.CO;2.

——, and C. S. Bretherton, 2009: The University of Washington shallow convection and moist turbulence schemes and their impact on climate simulations with the Community Atmosphere Model. *J. Climate,* **22,** 3449–3469, doi:10.1175/2008JCLI2557.1.

——, C. B. Leovy, and M. A. Rozendaal, 2004: A new heuristic Lagrangian marine boundary layer cloud model. *J. Atmos. Sci.,* **61,** 3002–3024, doi:10.1175/JAS-3344.1.

——, C. Bretherton, and P. Rasch, 2014: Integrating cloud processes in the Community Atmosphere Model, version 5. *J. Climate,* **27,** 6821–6856, doi:10.1175/JCLI-D-14-00087.1.

Saunders, P. M., 1961: An observational study of cumulus. *J. Meteor.,* **18,** 451–467, doi:10.1175/1520-0469(1961)018<0451:AOSOC>2.0.CO;2.

Siebesma, A. P., P. M. Soares, and J. Teixeira, 2007: A combined eddy-diffusivity mass-flux approach for the convective boundary layer. *J. Atmos. Sci.,* **64,** 1230–1248, doi:10.1175/JAS3888.1.

Simpson, J., and V. Wiggert, 1969: Models of precipitating cumulus towers. *Mon. Wea. Rev.,* **97,** 471–489, doi:10.1175/1520-0493(1969)097<0471:MOPCT>2.3.CO;2.

——, R. H. Simpson, D. A. Andrews, and M. A. Eaton, 1965: Experimental cumulus dynamics. *Rev. Geophys.,* **3,** 387–431, doi:10.1029/RG003i003p00387.

Song, X., and G. J. Zhang, 2009: Convection parameterization, tropical Pacific double ITCZ, and upper-ocean biases in the NCAR CCSM3. Part I: Climatology and atmospheric feedback. *J. Climate,* **22,** 4299–4315, doi:10.1175/2009JCLI2642.1.

Squires, P., 1958: Penetrative downdraughts in cumuli. *Tellus,* **10,** 381–389, doi:10.1111/j.2153-3490.1958.tb02025.x.

Stirling, A., and R. Stratton, 2012: Entrainment processes in the diurnal cycle of deep convection over land. *Quart. J. Roy. Meteor. Soc.,* **138,** 1135–1149, doi:10.1002/qj.1868.

Tiedtke, M., 1989: A comprehensive mass flux scheme for cumulus parameterization in large-scale models. *Mon. Wea. Rev.,* **117,** 1779–1800, doi:10.1175/1520-0493(1989)117<1779:ACMFSF>2.0.CO;2.

Turner, J., 1962: The starting plume in neutral surroundings. *J. Fluid Mech.,* **13,** 356–368, doi:10.1017/S0022112062000762.

Watanabe, M., and Coauthors, 2010: Improved climate simulation by MIROC5: Mean states, variability, and climate sensitivity. *J. Climate,* **23,** 6312–6335, doi:10.1175/2010JCLI3679.1.

Williamson, D. L., 2013: The effect of time steps and time-scales on parameterization suites. *Quart. J. Roy. Meteor. Soc.,* **139,** 548–560, doi:10.1002/qj.1992.

WMO, 1975: Manual on the observation of clouds and other meteors: Volume I. WMO Publ. 407, 155 pp.

Wu, X., and M. Yanai, 1994: Effects of vertical wind shear on the cumulus transport of momentum: Observations and parameterization. *J. Atmos. Sci.,* **51,** 1640–1660, doi:10.1175/1520-0469(1994)051<1640:EOVWSO>2.0.CO;2.

Zhang, G. J., and N. A. McFarlane, 1995: Sensitivity of climate simulations to the parameterization of cumulus convection in the Canadian Climate Centre general circulation model. *Atmos.–Ocean,* **33,** 407–446, doi:10.1080/07055900.1995.9649539.